Table II. Eighty-five genes expressed in the cancer patient-derived colonocytes but not in the healthy volunteer-derived colonocytes.

No.	Gene symbol	Gene title	Entrez gene ID	No expression in the PB
1	JUND	jun D proto-oncogene	3727	
2	TPT1	tumor protein, translationally-controlled 1	7178	*
3	RPL41	ribosomal protein L41	6171	*
4	RPS11	ribosomal protein S11	6205	*
5	RPS29	ribosomal protein S29	6235	*
6	RPL38	ribosomal protein L38	6169	*
7	SEPP1	selenoprotein P, plasma, 1	6414	*
8	RPL23	ribosomal protein L23	9349	*
9	B2M	ß-2-microglobulin	567	*
10	CFL1	cofilin 1 (non-muscle)	1072	*
11	RPL31	ribosomal protein L31	6160	*
12	RPS3A	ribosomal protein S3A	6189	
13	TMSB10	thymosin, ß 10	9168	*
14	RPL39	ribosomal protein L39	6170	*
15	HMGB1	high-mobility group box 1	3146	*
16	CEACAM6	carcinoembryonic antigen-related cell adhesion molecule 6 (non-specific cross reacting antigen)	4680	
17	ATP1B1	ATPase, Na^+/K^+ transporting, ß 1 polypeptide	481	*
18	RPS20	ribosomal protein S20	6224	*
19	ARF6	ADP-ribosylation factor 6	382	*
20	RPS21	ribosomal protein S21	6227	*
21	EIF5A	Eukaryotic translation initiation factor 5A	1984	*
22	RPL30	ribosomal protein L30	6156	*
23	EEF1A1	eukaryotic translation elongation factor 1 α 1	1915	*
24	RPL23A	ribosomal protein L23a	6147	*
25	LOC56902	putatative 28 kDa protein	56902	
26	RPL27	ribosomal protein L27	6155	*
27	SFN	stratifin	2810	*
28	CEACAM5	carcinoembryonic antigen-related cell adhesion molecule 5	1048	*
29	RPS24	ribosomal protein S24 /// ribosomal protein S24	6229	*
30	MARCKS	Myristoylated alanine-rich protein kinase C substrate	4082	*
31	PDE4C	phosphodiesterase 4C, cAMP-specific (phosphodiesterase E1 dunce homolog, *Drosophila*)	5143	
32	LOC651423	similar to mitogen-activated protein kinase kinase 3 isoform A	651423	
33	RPS10	ribosomal protein S10	6204	
34	CEP27	centrosomal protein 27 kDa	55142	
35	IL1RN	interleukin 1 receptor antagonist	3557	*
36	SLC35E1	solute carrier family 35, member E1	79939	
37	RPS27	ribosomal protein S27 (metallopanstimulin 1)	6232	*
38	RPS19	ribosomal protein S19	6223	*
39	RPS16	ribosomal protein S16	6217	*
40	MORF4L2	mortality factor 4 like 2	9643	*
41	RPL22	ribosomal protein L22	6146	*
42	RPS2	ribosomal protein S2	6187	*
43	RPLP2	ribosomal protein, large, P2	6181	*
44	RPL7A	ribosomal protein L7a	6130	
45	RPL7	ribosomal protein L7	6129	
46	RPS18	ribosomal protein S18	6222	*
47	HNRPH1	Heterogeneous nuclear ribonucleoprotein H1 (H)	3187	*
48	ZNF160	zinc finger protein 160	90338	

Table II. Continued.

No.	Gene symbol	Gene title	Entrez gene ID	No expression in the PB
49	RPS25	ribosomal protein S25	6230	*
50	PGF	Placental growth factor, vascular endothelial growth factor-related protein	5228	
51	SPG21	spastic paraplegia 21 (autosomal recessive, Mast syndrome)	51324	
52	RPL9	ribosomal protein L9	6133	*
53	PLEKHA5	Pleckstrin homology domain containing, family A member 5	54477	
54	PRR11	proline rich 11	55771	
55	CTNNB1	catenin (cadherin-associated protein), ß 1, 88 kDa	1499	*
56	NFKBIA	nuclear factor of κ light polypeptide gene enhancer in B-cells inhibitor, α	4792	*
57	GTSE1	G-2 and S-phase expressed 1	51512	
58	ATP8B1	ATPase, Class I, type 8B, member 1	5205	
59	TMED2	transmembrane emp24 domain trafficking protein 2	10959	*
60	RPS4X	ribosomal protein S4, X-linked	6191	
61	MUC3B	mucin 3B, cell surface associated	57876	
62	TTLL12	tubulin tyrosine ligase-like family, member 12	23170	
63	FTL	ferritin, light polypeptide	2512	*
64	TSPAN13	Tetraspanin 13	27075	*
65	PTP4A2	protein tyrosine phosphatase type IVA, member 2	8073	*
66	EGLN3	egl nine homolog 3 (C. elegans)	112399	*
67	ROCK2	Rho-associated, coiled-coil containing protein kinase 2	9475	
68	NDRG1	N-myc downstream regulated gene 1	10397	*
69	GTPBP1	GTP binding protein 1	9567	*
70	CAPZA1	capping protein (actin filament) muscle Z-line, α 1	829	*
71	RPL13	ribosomal protein L13	6137	*
72	CIDEC	cell death-inducing DFFA-like effector c	63924	*
73	SIRT3	sirtuin (silent mating type information regulation 2 homolog) 3 (S. cerevisiae)	23410	
74	LAPTM4A	lysosomal-associated protein transmembrane 4 α	9741	*
75	NOS1	nitric oxide synthase 1 (neuronal)	4842	*
76	COQ10B	coenzyme Q10 homolog B (S. cerevisiae)	80219	*
77	SAT	spermidine/spermine N1-acetyltransferase	6303	*
78	C1orf107	chromosome 1 open reading frame 107	27042	
79	TXN	thioredoxin	7295	*
80	SLC7A1	solute carrier family 7 (cationic amino acid transporter, y^+ system), member 1	6541	
81	SLC1A7	solute carrier family 1 (glutamate transporter), member 7	6512	
82	VIL2	villin 2 (ezrin)	7430	*
83	NTRK2	neurotrophic tyrosine kinase, receptor, type 2	4915	
84	GSTA1	Glutathione S-transferase A1	2938	
85	PTP4A3	protein tyrosine phosphatase type IVA, member 3	11156	

(•) Genes that were expressed in the cancer patient-derived colonocytes but not in either the healthy volunteer-derived colonocytes or the peripheral blood (PB) mixture.

peripheral blood, and squamous cells are potentially good markers for the screening of colorectal cancer from the feces. To identify effective genes for fecal RNA-based screening, we first compared 10 gene expression profiles of 6 early colorectal cancer tissues (2 Dukes stage A and 4 Dukes stage B cases), 3 advanced cancer RNA mixtures (6, 6, and 7 Dukes stage C or D cases), and a normal colorectal mucosa RNA mixture (6 cases). Of 14,564 genes, 2,926 were identified as genes which were not detected in the normal mucosa but detected in at least one of the above 9 cancer samples. Among these 2,926 cancer-specific genes, 205 genes, which were expressed in all of the 3 advanced cancer mixtures, were identified; however, only 3 genes were found to be expressed in all of the 6 early cancers. The cause of these results may

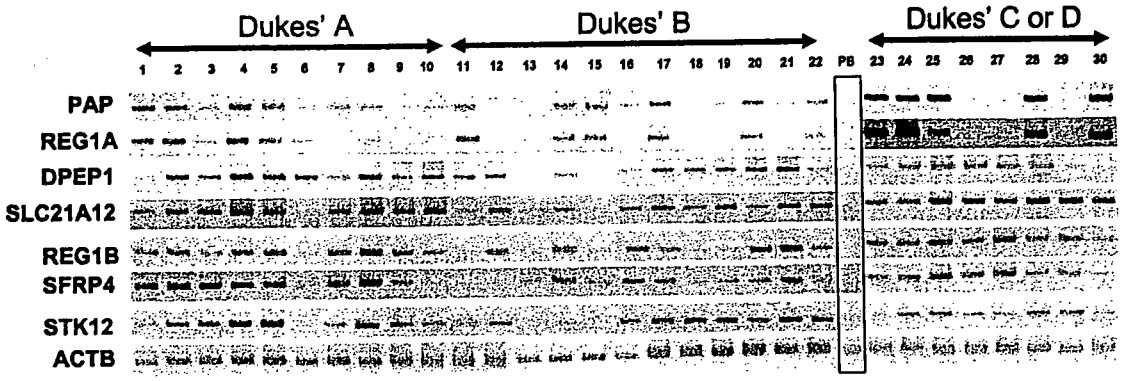

Figure 1. Results of RT-PCR of 7 genes (PAP, REG1A, DPEEP1, SLC21A12, REG1B, SFRP4, and STK12) selected by microarray analysis on 30 colorectal cancer tissues and on a peripheral blood mixture (PB). By microarray analyses, we first identified 15 genes which were expressed not in the normal colorectal mucosa mixture or in a peripheral blood mixture but in more than 4 of 6 early cancers (Dukes stage A or B) and in all of 3 advanced cancer mixtures (Dukes stage C or D). Next, we examined the frequency of the expression of these 15 genes in 30 colorectal cancer tissues (10 Dukes stage A, 12 Dukes stage B, and 8 Dukes stage C or D cancers), and selected, by RT-PCR, 7 genes (PAP, REG1A, DPEP1, SLC21A12, REG1B, SFRP4, and STK12) as the frequently expressed genes at any stage of colorectal cancer.

be that the expression profile of early cancer varies from case to case. Of 14,564 genes, we were able to select 65 genes which were expressed not in the normal colorectal mucosa mixture but in more than 4 of the 6 early cancers and in all of the 3 advanced cancer mixtures.

Considering bleeding by nonmalignant diseases such as hemorrhoids, which often give false positives in fecal colorectal cancer screening, we selected 15 genes from the 65 genes, because the expression of all the other 50 genes was detectable in a peripheral blood mixture of 58 healthy volunteers when a highly sensitive nested RT-PCR analysis with outer and inner primer sets was performed (data not shown). Next, we examined the frequency of the expression of these 15 genes in 30 colorectal cancer tissues (10 Dukes stage A, 12 Dukes stage B, and 8 Dukes stage C or D cancers), and selected, by RT-PCR, 7 genes (PAP, REG1A, DPEP1, SLC21A12, REG1B, SFRP4, and STK12) as the frequently expressed genes at any stage of colorectal cancer (Fig. 1). By RT-PCR, we lastly checked the expression of these 7 genes in RNA samples of the colonocytes of 15 healthy volunteers, which were isolated from the feces by FMCI (23). No mRNA expression of 3 genes (PAP, REG1A, and DPEP1) was detected in the colonocyte samples of all the 15 healthy volunteers; however, the other 4 genes (SLC21A12, REG1B, SFRP4, and STK12) were found to be expressed in some samples (data not shown). This fact may be due to the contamination of anal squamous cells, which were dissociated from the anus and survived in the feces, because our gene selection process can minimize the effect on the contamination of lymphocytes, red blood cells and dissociated normal colorectal epithelium. Under the above criteria, only 3 genes were selected as the final candidates for the fecal RNA-based early detection of colorectal cancer.

Marker gene selection by comparison of expression profiles between healthy volunteer- and cancer patient-derived colonocytes from the feces. Next, we obtained and compared 5 gene expression profiles of 4 colonocyte RNA samples (CF15, CF17, CF18, and CF25), which were isolated from the feces of 4 colorectal cancer patients by FMCI, and a colonocyte RNA mixture (HVF) of 7 healthy volunteers. Of 14,564 genes, the number of detectable genes in 5 colonocyte samples, CF15, CF17, CF18, CF25, and HVF is 768, 603, 772, 459, and 326, respectively. The number of detectable genes in the colonocyte is approximately 6.5% of that (11,343) in the colorectal cancer tissue. The major reason seems to be that most colonocytes are not in the cell division cycle but are resting, because the detectable gene number (1,535) in the peripheral blood composing such resting cells was also small. Unexpectedly, 716 (93%), 553 (92%), 712 (92%), and 424 (92%) of the above detectable genes (768, 603, 772, and 459) in the the colonocytes of the cancer patients were not expressed in those of the healthy volunteers. The huge difference of the colonocyte expression profiles between the colorectal cancer patients and the healthy volunteers might lead to success in gene selection for fecal RNA-based early detection of colorectal cancer. Eighty-five genes, whose expression was found in 3 or 4 of the 4 colorectal cancer patient samples (CF15, CF17, CF18, and CF25) but not in the HVF, were identified (Table II). Of these 85 genes, 29 (34%) were found to encode ribosomal proteins (RPLs or RPSs). In the course of a series of studies, it is predicted that normal mucous cells will die and be exfoliated during turnover and that the colorectal cancer cells will survive for a long time in the isolation processes as well as in the feces (22,23). Therefore, protein synthesis in the cells would be maintained actively for cancer cell survival under these conditions. The FMCI can minimize the contamination of both lymphocytes and red blood cells because the FMCI contains the enrichment process of epithelial cells such as colorectal cancer cells, the contaminated anal squamous cells, and a few living cells dissociated from the normal colorectal mucosa by MACS (23). Therefore, expression status in the peripheral blood is not needed for the gene selection process for fecal RNA-based screening; all of the 85 genes are expected to be good markers if the colonocytes are isolated by FMCI.

RT-PCR and focused microarray analyses of 9 selected genes in 30 colonocyte RNA samples. Next, we performed RT-PCR of the first 3 identified genes (PAP, REG1A, and DPEP1) in the colonocyte RNA samples which were prepared from 23 curable colorectal cancer patients (Dukes stages A-C) and 7 healthy volunteers. The 23 colorectal cancer patients were 8

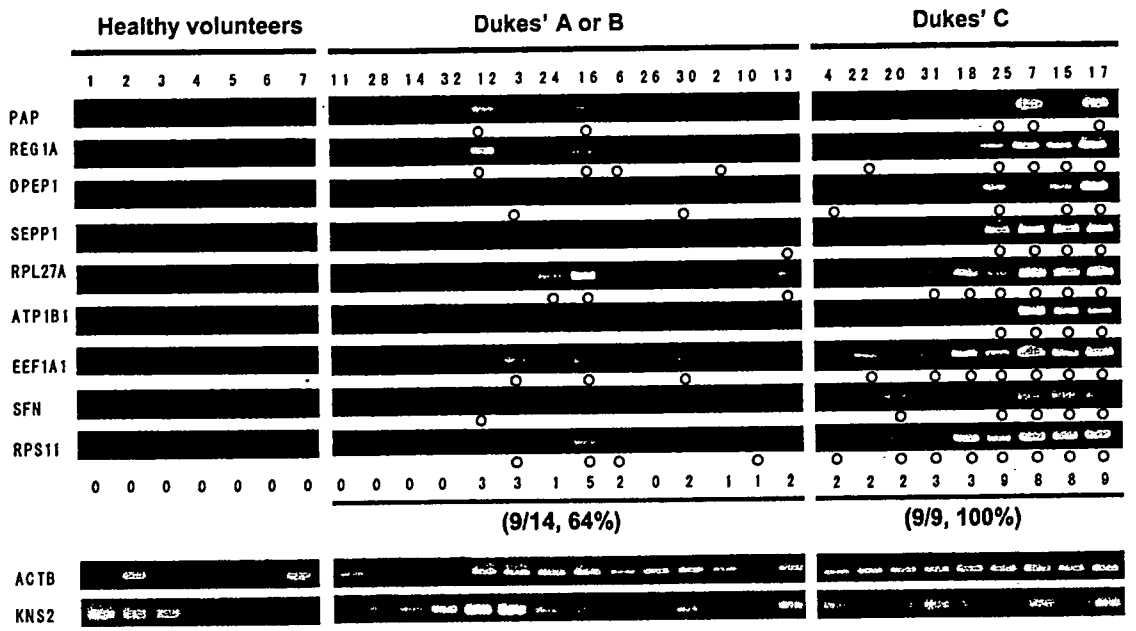

Figure 2. Results of RT-PCR of 9 genes (PAP, REG1A, DPEEP1, SEPP1, RPL27A, ATP1B1, EEF1A1, SFN, and RPS11) in the colonocyte RNA samples from 23 curable colorectal cancer patients and 7 healthy volunteers. We performed RT-PCR of the first 3 identified genes (PAP, REG1A, and DPEP1) in the colonocyte RNA samples which were prepared from 23 curable colorectal cancer patients (8 Dukes stage A, 6 Dukes stage B, and 9 Dukes stage C) and 7 healthy volunteers. Next, to test the power of the 85 genes, which were identified by colonocyte gene expression profiling, we randomly selected 6 (SEPP1, RPL27A, ATP1B1, EEF1A1, SFN, and RPS11), and performed RT-PCR on the same samples. In total, RT-PCR of those 9 genes detected 18 (78%) of the 23 cancer patients, and 9 (64%) of the 14 early cancers (Dukes stage A or B) were detected; however, the expression of all of the 7 genes was hardly detected in the 7 healthy volunteers (upper panel). The expression level of housekeeping genes such as ACTB (ß-actin) was highly varied from sample to sample (lower panel). KNS2 encoding kinesin 2 was selected, by microarray analyses, as a gene expressed constantly in any colonocyte RNA sample; however, the expression level was also varied. Open circles indicate positive RT-PCR product, and numbers indicate the number of the positive genes in each sample.

with Dukes stage A, 6 with Dukes stage B, and 9 with Dukes stage C cancers; 5 were right-sided and 18 were left-sided cancers. Twelve (52%) of the 23 cancers were positive by RT-PCR in at least one of the 3 genes whereas no positive gene was found in any of the healthy volunteers (Fig. 2). To test the power of the 85 genes, which were identified by colonocyte gene expression profiling, we randomly selected 6 (SEPP1, RPL27A, ATP1B1, EEF1A1, SFN, and RPS11). RT-PCR of these 6 genes detected 16 (70%) of the 23 cancers as at least positive for 1 gene whereas no positive gene was found in any of the healthy volunteers (Fig. 2). No or a quite low signal of all the 9 genes was found in another RT-PCR experiment with 8 healthy volunteers (data not shown). In total, RT-PCR of those 9 genes detected 18 (78%) of the 23 cancer patients (Fig. 2). The 18 patients detected were 4 with Dukes stage A, 5 with Dukes stage B, and 9 with Dukes stage C cancers; 4 were right-sided and 14 were left-sided cancers. Therefore, 9 (64%) of the 14 early cancers (Dukes stage A or B), which have no lymph node metastasis, and show a good prognosis, were able to be detected. Importantly, 4/5 (80%) of the right-sided colorectal cancers were detected, which have been reported to be very difficult to detect by any feces-based molecular biological method, because most right-sided cancer-derived colonocytes are severely damaged from remaining for a long time in the feces.

For fecal RNA-based detection of early colorectal cancer, quantitative real-time RT-PCR is thought to hardly apply in the colonocyte because the expression level of housekeeping genes was highly varied from sample to sample (Fig. 2). The expressional variation could be explained by the difference of the physiological condition of colorectal cancer cells and anal squamous cells isolated from the feces by FMCI. All of the 9 genes were selected as cancer cell- or cancer patient-derived colonocyte-specific genes. Therefore, a negative or positive assay was thought to be sufficient for fecal RNA-based colorectal cancer detection. Accordingly, we developed a multiplex RT-PCR-based microarray assay for evaluating the above RT-PCR results and for providing an effective imaging tool for mass cancer screenings (Fig. 3). The Cy3-labeled cDNAs prepared by multiplex RT-PCR in a single tube were hybridized with 9 gene sequences on a focused microarray, which was manufactured by our previously developed Bubble Jet Technology with a small modification (25). Hybridization signals and the number of positive genes in the above 23 cancer patient-derived colonocyte RNA samples and 7 healthy volunteer-derived colonocyte RNA samples are shown in Fig 4. In total, a high concordance was observed between the focused microarray and RT-PCR. The focused microarray detected 18 (78%) of the 23 cancer patients. Ten (71%) of the 14 early cancers (Dukes stage A or B) and 4 (80%) of the 5 right-sided cancers were detected.

Discussion

Although the number of samples examined in this study is considered to be small, the evidence suggests that these successful results could be obtained from the high-quality of the RNA of the colonocytes, which were isolated by FMCI. From a practical point of view for mass cancer screenings, it is noted that the same number of colonocytes from fecal

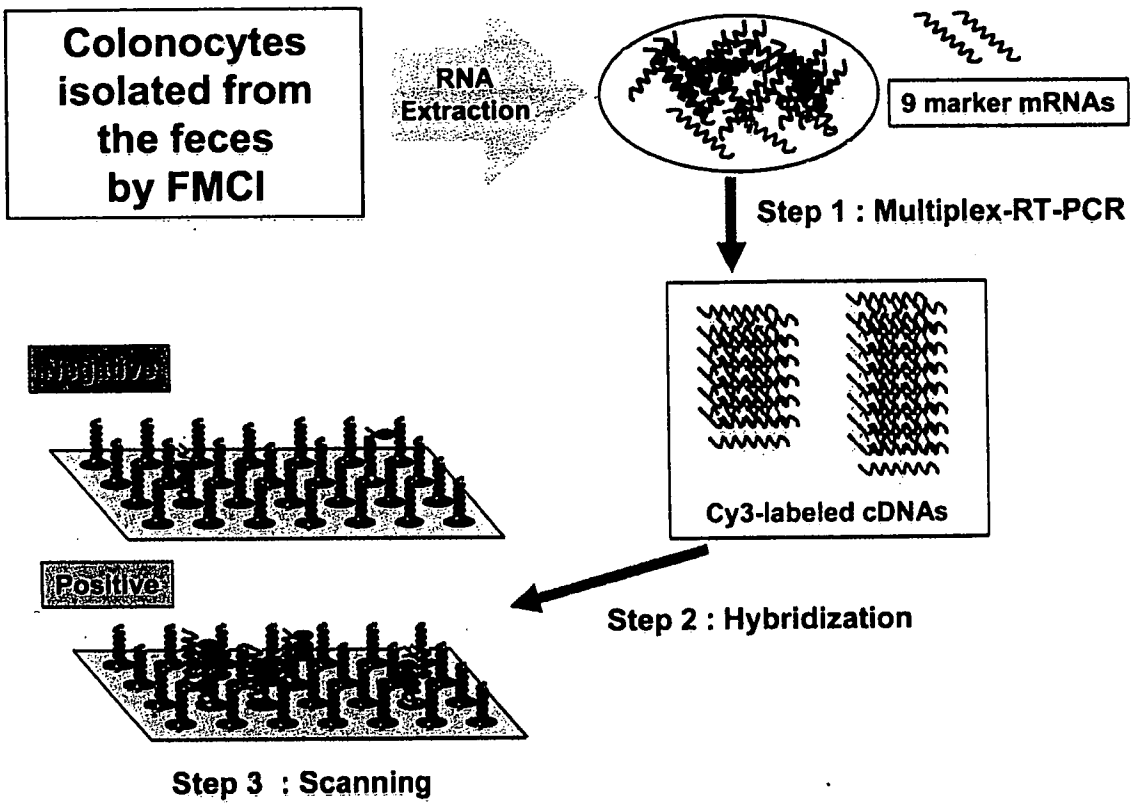

Figure 3. Schematic flow diagram of a focused micoarray assay. Marker mRNAs (PAP, REG1A, DPEP1, SEPP1, RPL27A, ATP1B1, EEF1A1, SFN, and RPS11 mRNAs) were amplified and labeled with Cy3-dUTP by multiplex-RT-PCR among total RNAs from colonocytes isolated by FMCI (step 1) and hybridized to focused micoarray (step 2), followed by fluorescence intensity scanning (step 3).

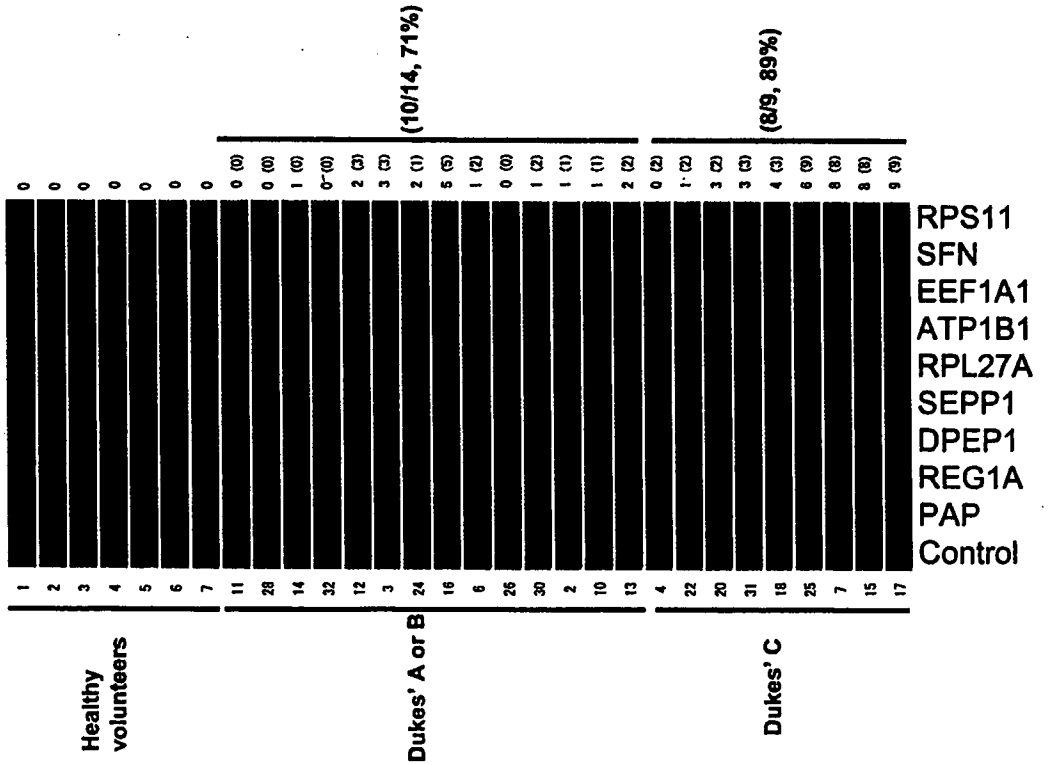

Figure 4. Hybridization image of focused microarray analysis and the number of positive genes in 30 colonocyte RNA samples. The Cy3-labeled cDNAs prepared by multiplex RT-PCR in two tubes were hybridized with 9 gene sequences (PAP, REG1A, DPEP1, SEPP1, RPL27A, ATP1B1, EEF1A1, SFN, and RPS11) on a focused microarray, which was manufactured by our previously developed Bubble Jet Technology with a small modification (25). Hybridization signals and the number of positive genes (right) in the above 23 cancer patient-derived colonocyte RNA samples and 7 healthy volunteer-derived colonocyte RNA samples are shown. In total, a high concordance was observed between focused microarray and RT-PCR. Ten (71%) of the 14 early cancers (Dukes stage A or B) and 8 (89%) of 9 Dukes stage C cancers were detected by the focused microarray analysis. The number of positive genes in RT-PCR are in parentheses (Fig. 2).

materials 6 h to 3 days after evacuation can be obtained if the feces are kept at 4°C (23). However, if conventional fecal RNA preparation methods without the epithelial cell enrichment process are used for colorectal cancer screening, we have to consider the contamination of blood in the feces, which derives from nonmalignant diseases. Considering the use of such methods, to this end we further provided 56 genes, which were expressed in the cancer patient-derived colonocytes but not in either the healthy volunteer-derived colonocytes or the peripheral blood mixture (Table II). This study suggests that the fecal RNA-based method could be a promising procedure for the detection of early or right-sided colorectal cancers. We recently developed a very effective focused microarray assay for detecting minimal gastric cancer cells in peritoneal washings, demonstrating a specificity and sensitivity equal to or better than cytology in two large specialist hospitals with trained cytologists (26). Therefore, the focused microarray assay could provide an effective imaging tool for mass screening, and our extensive gene list provides useful markers.

Acknowledgments

This study was supported in part by the program for promotion of Fundamental Studies in Health Sciences of the National Institute of Biomedical Innovation (NiBio); in part by a Grant-in-Aid for the Third Comprehensive 10-Year Strategy for Cancer Control and for Cancer Research (16-15) from the Ministry of Health, Labour and Welfare of Japan, and in part by a research and development project of the Industrial Science and Technology Program supported by the New Energy and Industrial Technology Development Organization (NEDO) of Japan. We thank Ayako Nomura and Megumi Sato for their excellent assistance with primer design for RT-PCR.

References

1. Mandel JS, Bond JH, Church TR, Snover DC, Bradley GM, Schman LM and Ederer F: Reducing mortality from colorectal cancer by screening for fecal occult blood. Minnesota Colon Cancer Control Study. N Engl J Med 328: 1365-1371, 1993.
2. Hardcastle JD, Chamberlain JO, Robinson MH, Moss SM, Amar SS, Balfour TW, James PD and Mangham CM: Randomised controlled trial of faecal-occult-blood screening for colorectal cancer. Lancet 348: 1472-1477, 1996.
3. Kronborg O, Fenger C, Olson J, Jorgensen OD and Sondergaard O: Randomized study of screening for colorectal cancer with faecal-occult-blood test. Lancet 348: 1467-1471, 1996.
4. Towler B, Irwig L, Glasziou P, Kewenter J, Weller D and Silagy C: A systematic review of the effects of screening for colorectal cancer using the faecal occult blood test, hemoccult. BMJ 317: 559-565, 1998.
5. Winawer S, Fletcher R, Rex D, Bond J, Burt R, Ferucci J, Ganiats T, Levin T, Woolf S, Johnson D, Kirk L, Litin S and Simmang C: Colorectal cancer screening and surveillance: clinical guidelines and rationale-update based on new evidence. Gastroenterology 124: 544-560, 2003.
6. Mandel JS, Church TR, Bond JH, Ederer F, Geisser MS, Mongin SJ, Snover DC and Schuman LM: The effect of fecal occult-blood screening on the incidence of colorectal cancer. N Engl J Med 343: 1603-1607, 2000.
7. Sidransky D, Tokino T, Hamilton SR, Kinzler KW, Levin B, Frost P and Vogelstein B: Identification of ras oncogene mutations in the stool of patients with curable colorectal tumors. Science 256: 102-105, 1992.
8. Hasegawa Y, Takeda S, Ichii S, Koizumi K, Maruyama M, Fujii A, Ohta H, Nakajima T, Okuda M, Baba S, *et al*: Detection of K-ras mutations in DNAs isolated from feces of patients with colorectal tumors by mutant-allele-specific amplification (MASA). Oncogene 10: 1441-1445, 1995.
9. Smith-Ravin J, England J, Talbot IC and Bodmer W: Detection of c-Ki-ras mutations in faecal samples from sporadic colorectal cancer patients. Gut 36: 81-86, 1995.
10. Eguchi S, Kohara N, Komuta K and Kanematsu T: Mutations of the p53 gene in the stool of patients with resectable colorectal cancer. Cancer 77: 1707-1710, 1996.
11. Nollau P, Moser C, Weinland G and Wagener C: Detection of K-ras mutations in stools of patients with colorectal cancer by mutant-enriched PCR. Int J Cancer 66: 332-336, 1996.
12. Ratto C, Flamini G, Sofo L, Nusera P, Ippliti M, Curigliano G, Ferreti G, Sgambato A, Merico M, Doglietto GB, Cittadini A and Crucitti F: Detection of oncogene mutation from neoplastic colonic cells exfoliated in feces. Dis Colon Rectum 39: 1238-1244, 1996.
13. Deuter R and Muller O: Detection of APC mutations in stool DNA of patients with colorectal cancer by HD-PCR. Hum Mutat 11: 84-89, 1998.
14. Ahlquist DA, Skoletsky JE, Boynton KA, Harrington JJ, Mahoney DW, Pierceall WE, Thibodeau SN and Shuber AP: Colorectal cancer screening by detection of altered human DNA in stool: feasibility of a multitarget assay panel. Gastroenterology 119: 1219-1227, 2000.
15. Dong SM, Traverso G, Johnson C, Geng L, Favis R, Boynton K, Hibi K, Goodman SN, D'Allessio M, Paty P, Hamilton SR, Sidransky D, Barany F, Levin B, Shuber A, Kinzler KW, Vogelstein B and Jen J: Detecting colorectal cancer in stool with the use of multiple genetic targets. J Natl Cancer Inst 93: 858-865, 2001.
16. Rengucci C, Maiolo P, Saragoni L, Zoli W, Amadori D and Calistri D: Multiple detection of genetic alterations in tumors and stool. Clin Cancer Res 7: 590-593, 2001.
17. Traverso G, Shuber A, Olsson L, Levin B, Johnson C, Hamilton SR, Boynton K, Kinzler KW and Vogelstein B: Detection of proximal colorectal cancers through analysis of faecal DNA. Lancet 359: 403-404, 2002.
18. Traverso G, Shuber A, Levin B, Levin B, Johnson C, Hamilton SR, Boynton K, Kinzler KW and Vogelstein B: Detection of APC mutations in fecal DNA from patients with colorectal tumors. N Engl J Med 346: 311-320, 2002.
19. Boynton KA, Summerhayes IC, Ahlquist DA and Shuber AP: DNA integrity as a potential marker for stool-based detection of colorectal cancer. Clin Chem 49: 1058-1065, 2003.
20. Matsumura Y and Tarin D: Significance of CD44 gene products for cancer diagnosis and disease evaluation. Lancet 340: 1053-1058, 1992.
21. Mastumura Y, Hanbury D, Smith J and Tarin D: Non-invasive detection of malignancy by identification of unusual CD44 gene activity in exfoliated cancer cells. BMJ 308: 619-624, 1994.
22. Yamao T, Matsumura Y, Shimada Y, Moriya Y, Sugihara K, Akasu T, Fujita S and Kakizoe T: Abnormal expression of CD44 variants in the exfoliated cells in the feces of patients with colorectal cancer. Gastroenterology 114: 1196-1205, 1998.
23. Matsushita H, Matsumura Y, Moriya Y, Akasu T, Fujita S, Yamamoto S, Onouchi S, Saito N, Sugito M, Ito M, Kozu T, Minowa T, Nomura S, Tsunoda H and Kakizoe T: A new method for isolating colonocytes from naturally evacuated feces and its clinical application to colorectal cancer diagnosis. Gastroenterology 129: 1918-1927, 2005.
24. Mori K, Aoyagi K, Ueda T, Danjoh I, Tsubosa Y, Yanagihara K, Matsuno Y, Sasako M, Sakamoto H, Mafune K, Kaminishi M, Yoshida T, Terada M and Sasaki H: Highly specific marker genes for detecting minimal gastric cancer cells in cytology negative peritoneal washings. Biochem Biophys Res Commun 313: 931-937, 2004.
25. Okamoto T, Suzuki T and Yamamoto N: Microarray fabrication with covalent attachment of DNA using Bubble Jet Technology. Nat Biotech 18: 438-441, 2000.
26. Mori K, Suzuki T, Uozaki H, Nakanishi H, Ueda T, Matsuno Y, Kodera Y, Sakamoto H, Yamamoto N, Sasako M, Kaminishi M and Sasaki H: Detection of minimal gastric cancer cells in peritoneal washings by focused microarray analysis with multiple markers: clinical implications. Ann Surg Oncol 14: 1694-1702, 2007.

Novel SN-38–Incorporated Polymeric Micelle, NK012, Strongly Suppresses Renal Cancer Progression

Makoto Sumitomo,[1] Fumiaki Koizumi,[2] Takako Asano,[1] Akio Horiguchi,[1] Keiichi Ito,[1] Tomohiko Asano,[1] Tadao Kakizoe,[3] Masamichi Hayakawa,[1] and Yasuhiro Matsumura[4]

[1]Department of Urology, National Defense Medical College, Tokorozawa, Saitama, Japan; [2]Shien-Lab, Medical Oncology, National Cancer Center Hospital; [3]National Cancer Center, Tokyo, Japan; and [4]Investigative Treatment Division, Research Center for Innovative Oncology, National Cancer Center Hospital East, Chiba, Japan

Abstract

It has been recently reported that NK012, a 7-ethyl-10-hydroxy-camptothecin (SN-38)–releasing nanodevice, markedly enhances the antitumor activity of SN-38, especially in hypervascular tumors through the enhanced permeability and retention effect. Renal cell carcinoma (RCC) is a typical hypervascular tumor with an irregular vascular architecture. We therefore investigated the antitumor activity of NK012 in a hypervascular tumor model from RCC. Immunohistochemical examination revealed that Renca tumors contained much more CD34-positive neovessels than SKRC-49 tumors. Compared with CPT-11, NK012 had significant antitumor activity against both bulky Renca and SKRC-49 tumors. Notably, NK012 eradicated rapid-growing Renca tumors in 6 of 10 mice, whereas it failed to eradicate SKRC-49 tumors. In the pulmonary metastasis treatment model, an enhanced and prolonged distribution of free SN-38 was observed in metastatic lung tissues but not in nonmetastatic lung tissues after NK012 administration. NK012 treatment resulted in a significant decrease in metastatic nodule number and was of benefit to survival. Our study shows the outstanding advantage of polymeric micelle-based drug carriers and suggests that NK012 would be effective in treating disseminated RCCs with irregular vascular architectures. [Cancer Res 2008;68(6):1631–5]

Introduction

Passive targeting of the drug delivery system is suited to combating the pathophysiologic characteristics present in many solid tumors: hypervascularity, irregular vascular architecture, potential for secretion of vascular permeability factors, and the absence of effective lymphatic drainage that prevents efficient clearance of macromolecules. These characteristics, unique to solid tumors, are believed to be the basis of the enhanced permeability and retention (EPR) effect (1). Polymeric micelle-based anticancer drugs have recently been developed (2, 3), and some were put under evaluation for clinical trials (4, 5).

7-Ethyl-10-hydroxy-camptothecin (SN-38), a biological active metabolite of irinotecan hydrochloride (CPT-11), has potent antitumor activity, but has not been used clinically because it is a water-insoluble drug. It has been recently shown that novel SN38-incorporated polymeric micelles, NK012, have the potential to allow effective sustained release of SN-38 inside a tumor and possess potent antitumor activities especially in a vascular endothelial growth factor (VEGF)–secreting hypervascular tumor (6), because the supramolecular structures of NK012 which enable SN-38 to accumulate in the target tissue are based on the EPR effect (1).

Renal cell carcinoma (RCC) is a typical hypervascular tumor with an irregular vascular architecture. We therefore conducted an investigation to determine whether NK012 would be effective in treating RCC by using established RCC tumor models with pulmonary metastasis.

Materials and Methods

Drugs and cells. CPT-11 was purchased from Yakult Honsha Co., Ltd. SN-38 and NK012 was prepared and supplied by Nippon Kayaku Co., Ltd. (6). Five human RCC lines (SKRC-49, Caki-1, 769P, 786O, and KU19-20) and murine Renca cells were maintained in DMEM or MEM supplemented with 2 mmol/L glutamine, 1% nonessential amino acids, 100 units/mL streptomycin and penicillin, and 10% FCS.

***In vitro* growth inhibition assay.** The growth inhibitory effects of NK012, SN-38, and CPT-11 were examined with a 3-(4, 5-dimethylthiazol-2-yl)-2, 5-diphenyltetrazolium bromide (MTT) assay, as described previously (6).

***In vivo* growth inhibition assay.** The animal experimental protocols were approved by the Committee for Ethics of Animal Experimentation, and the experiments were conducted in accordance with the Guidelines for Animal Experiments in the National Cancer Center. Athymic nude mice (3–4 wk old) were maintained in a laminar air flow cabinet under aseptic conditions. 10^7 RCC cells were s.c. injected into the backs of the mice. NK012 at doses of 10 mg/kg/d or 20 mg/kg/d and CPT-11 at doses of 15 mg/kg/d or 30 mg/kg/d were given i.v. on days 0 (when tumors were allowed to grow until they became massive in size, around 1.5 cm), 4, and 8. Tumor volume was determined by direct measurement with calipers and calculated as $\pi/6 \times (\text{large diameter}) \times (\text{small diameter})^2$.

Assessment of treatment effects of NK012 on murine pulmonary metastasis model. A total of 1×10^5 Renca cells were inoculated into male BALB/c mice via the tail vein. The mice were randomly divided into three groups of 10. NK012 at dose of 20 mg/kg/d and CPT-11 at dose of 30 mg/kg/d were given i.v. on days 0 (7 d after inoculation), 4, and 8. After that, the mice were sacrificed, their lungs were stained intratracheally with 15% India black ink solution, and the number of metastatic nodules in each mouse was counted. To determine the effect of NK012 on survival, an identical experiment to the one described above was done. After treatment, mice were maintained until each animal showed signs of morbidity (i.e., over 10% weight loss compared with untreated controls), at which point they were sacrificed. Kaplan-Meier analysis was done to determine the effect on time to morbidity, and statistical differences were ranked according to a Mantel-Cox log-rank test using the StatView 5.0 software package.

Histologic and immunohistochemical analysis. Histologic sections were taken from Renca tumor tissues. After extirpation, tissues were fixed with 3.9% formalin in PBS (pH 7.4), and the subsequent preparations and H&E staining were performed by Tokyo Histopathological Laboratory Co.,

Requests for reprints: Yasuhiro Matsumura, Investigative Treatment Division, Research Center for Innovative Oncology, National Cancer Center Hospital East, 6-5-1 Kashiwanoha, Kashiwa City, Chiba 277-8577, Japan. Phone: 81-4-7134-6857; Fax: 81-4-7134-6857; E-mail: yhmatsum@east.ncc.go.jp.

doi:10.1158/0008-5472.CAN-07-6532

Table 1. *In vitro* growth inhibitory activity of SN-38, NK012, and CPT-11 in RCC lines (MTT assay)

Cell line	IC_{50} (μmol/L)		
	SN-38	NK012*	CPT-11
SKRC-49	0.0064 ± 0.005	0.011 ± 0.008	4.14 ± 0.45
Caki-1	0.0062 ± 0.009	0.032 ± 0.006	8.45 ± 0.85
769P	0.015 ± 0.007	0.085 ± 0.014	34.54 ± 3.76
786O	0.031 ± 0.007	0.12 ± 0.012	28.14 ± 1.21
KU19-20	0.10 ± 0.006	0.34 ± 0.014	32.65 ± 1.25
Renca	0045 ± 0.005	0.0096 ± 0.008	2.26 ± 0.05

*The dose of NK012 is expressed as a dose equivalent to SN-38.

Ltd. Monoclonal anti-CD34 antibody (HyCult Biotechnology) was used to detect the tumor blood vessels. CD34-positive neovessels were counted in 10 high-power fields (×400) by two independent investigators who operated in a blinded fashion.

Assay for free (polymer-unbound) SN-38 in lung tissues. The Renca pulmonary metastasis model described above was used for the analysis of the biodistribution of NK012 and CPT-11. Ten days after Renca inoculation, NK012 (20 mg/kg) or CPT-11 (30 mg/kg) was given i.v. to the mice. The mice were sacrificed at 0, 24, 48, and 72 h after administration, and lung samples were taken and stored at −80°C until analysis. We prepared control mice without Renca inoculation as the nonmetastatic model; NK012 was administrated as well, and lung samples were stored. Samples were then homogenized on ice using a Digital homogenizer (Iuchi) and suspended in the mixture of 100 mmol/L glycine-HCl buffer (pH 3)/methanol (1:1, v/v) at a concentration of 5% w/w. Proteins were precipitated with an ice-cold mixture of 1 mmol/L H_3PO_4/MeOH/H_2O (1:1:4, v/v/v) containing camptothecin as an I.S. The sample was vortexed for 10 s and filtered through a MultiScreen Solvinert (Millipore Corporation), and the concentration of free SN-38 in the aliquots of the homogenates (100 μL) was determined using the high-performance liquid chromatography method (6).

Statistical analysis. Data were expressed as mean ± SD. Significance of differences was calculated using the unpaired *t* test with repeated measures of StatView 5.0. $P < 0.05$ was regarded as statistically significant.

Results and Discussion

We first evaluated *in vitro* cellular sensitivity of RCC lines to SN-38, NK012, and CPT-11. The IC_{50} values of each agent for RCC lines are shown in Table 1. NK012 exhibited higher cytotoxic effect against each cell line compared with CPT-11 (96-fold to 406-fold sensitive).

It is essential to elucidate the correlation between the effectiveness of micellar drugs and tumor hypervascularity and hyperpermeability. Gross evaluation of those RCC tumors s.c. injected into the backs of mice revealed that Renca tumors were more reddish and grew faster than SKRC-49 tumors, and immunohistochemical examination showed that Renca tumors contained much more CD34-positive neovessels than SKRC-49 tumors (Fig. 1).

We allowed the tumors to grow until they became massive, around 1.5 cm, and then initiated treatment. A striking decrease in Renca tumor volume was observed on day 15 in mice treated with NK012 at 20 mg/kg/d compared with the untreated control (Fig. 2*A*). Renca bulky masses completely disappeared on day 21 in 6 of 10 mice treated with NK012 at 20 mg/kg/d. On the other hand, Renca tumors in mice treated with CPT-11 at 30 mg/kg/d were not eradicated and rapidly regrew after a partial response at day 15. An approximate 10% body weight loss occurred in mice treated with NK012 20 mg/kg, compared with the untreated controls, but there was no significant difference in comparison with tumor-free mice treated with NK012, suggesting that the decrease in body weight was likely to be due to tumor shrinkage rather than toxic effects. We next compared the antitumor activities of the NK012 and CPT-11 treatment in SKRC-49 and Renca tumors. The SKRC-49 tumor volume in mice treated with NK012 at 20 mg/kg/d on day 21 was over 70% smaller than in the untreated controls on day 21 and ~50% smaller than in mice on day 0 (Fig. 2*B*). However, the SKRC-49 tumors were not eradicated in mice treated with NK012. Considering that equivalent *in vitro* growth inhibitory effects by NK012 were observed for SKRC-49 and Renca cells (Table 1), our results suggest that the antitumor activity of NK012 *in vivo* might be affected by tumor environment factors, such as tumor vascularity.

We next examined the distribution of free SN-38 in the metastatic or nonmetastatic (no inoculation of Renca cells) lung tissues after administration of NK012 or CPT-11. In the case of NK012 administration in mice with lung metastasis, free SN-38 was detectable at the concentration of >100 ng/g in metastatic lung tissues with a typical microvascular architecture (Fig. 3*A*) even at 72 hours after administration, whereas the concentrations of free SN-38 in nonmetastatic lung tissues after NK012 administration were much lower than those in metastatic lung tissues after treatment with NK012 (significant at 24, 48, and 72 hours; $P < 0.05$;

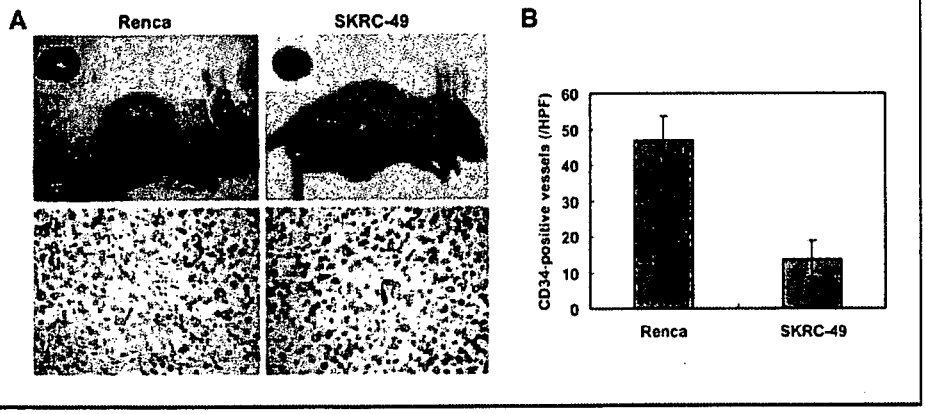

Figure 1. Comparison of tumor angiogeneses of Renca and SKRC-49 in athymic nude mice. *A*, representative photographs of massive tumors developed from Renca and SKRC-49 at 28 d after s.c. injection (inoculation). Immunohistochemical (CD34, ×400) examinations for each tumor are shown. *B*, tumor neovascularization in each tumor was quantified by counting CD34-positive neovessels. *Bars*, SD. Experiments were repeated twice with similar results.

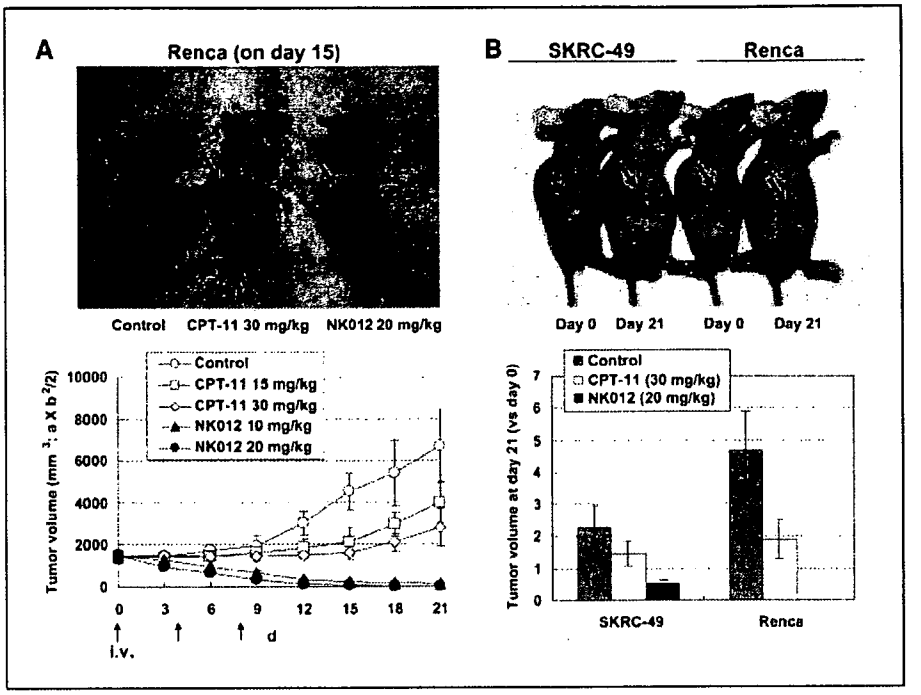

Figure 2. Growth-inhibitory effect of NK012 and CPT-11 on bulky RCC tumors. I.v. administration of NK012 or CPT-11 was started when the mean tumor volumes of groups reached a massive 1,500 mm^3. The mice were divided into test groups as indicated. *A*, representative of each group at day 15 in the Renca allograft model. *Arrows*, Renca allografts (*top*). Time profile of tumor volume in mice treated with NK012 or CPT-11 at indicated doses (*bottom*). Each group consisted of 10 mice. *Bars*, SD. *B*, the comparison of antitumor activities of CPT-11 and NK012 in SKRC-49 xenografts and Renca allografts. Representative of mice treated with NK012 at day 0 and day 21. Experiments were repeated twice with similar results. The mice at day 0 in the photograph belong to the group in the second experiment which started just at day 21 of the first experiment. *Arrows*, tumor grafts. The relative tumor volume values at day 21 to those at day 0 in each group set to 1 (*bottom*). Each group consisted of 10 mice.

Fig. 3*B*). On the other hand, the concentrations of free SN-38 after administration of CPT-11 were almost negligible in metastatic lung tissues at all time points (data not shown). These results strongly suggest that SN-38 could be selectively released from NK012 and maintained in metastatic Renca tumor tissues.

Deviating from the ordinary experimental pulmonary metastasis prevention model, we initiated treatment 7 days after inoculation (day 0) when multiple lung nodules derived from Renca were observed in all mice in our preliminary study (Fig. 4*A*). On day 21, there was no significant difference between the mean number of metastatic nodules in the control group (287 ± 56 nodules, $n = 10$) and in the group receiving CPT-11 treatment (236 ± 59 nodules, $n = 10$). Significant treatment effects were found, however, in the group receiving NK012 treatment (32 ± 18 nodules, $n = 10$) on day 21 compared with the control group on day 21 ($P < 0.0001$). Notably, a dramatic decrease in metastatic nodule number was observed in the NK012 treatment group on day 21 compared with the control group on day 0 (126 ± 23 nodules, $n = 10$, $P < 0.001$; Fig. 4*A*). Kaplan-Meier analysis showed that a significant survival benefit was obtained in the NK012 treatment group compared with

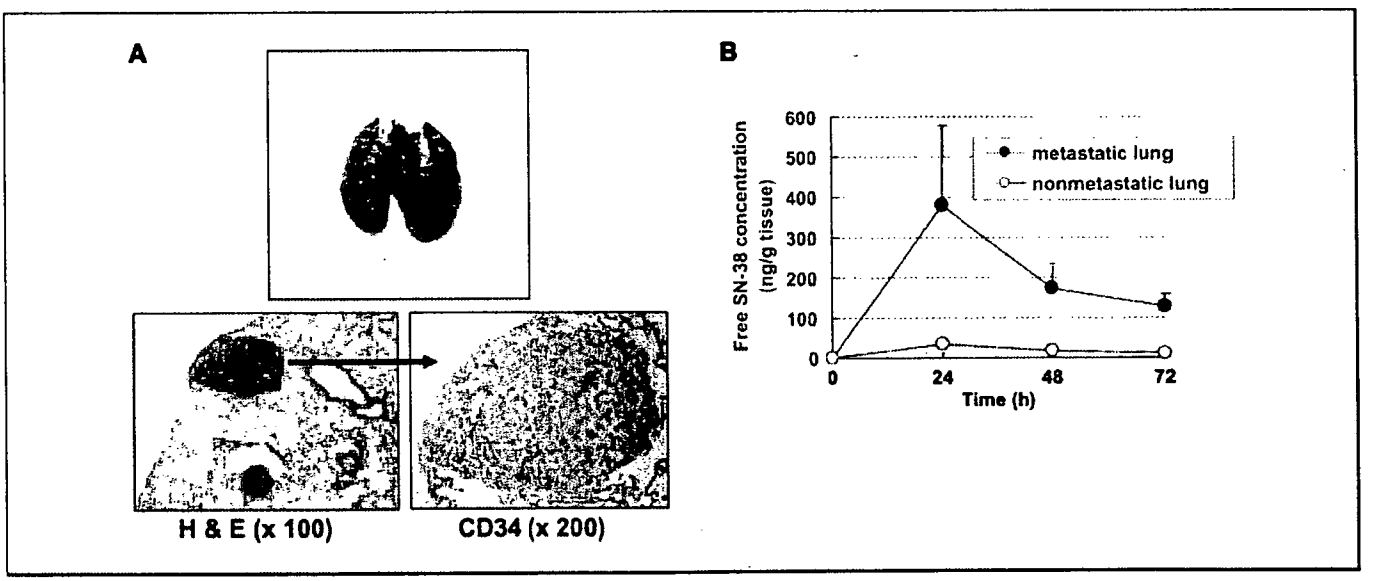

Figure 3. Pulmonary metastasis of Renca cells and lung tissue distribution of free SN-38 after administration of NK012 and CPT-11. *A*, gross appearances of pulmonary metastasis observed 7 d after Renca inoculation (*top*). Multiple metastatic nodules and neovascularization in metastatic lung tumor lesion (*bottom*). *B*, time profile of free SN-38 concentration in metastatic or nonmetastatic lung tissues in mice treated with NK012 (20 mg/kg/d). *Bars*, SD. Experiments were performed in tetraplicate.

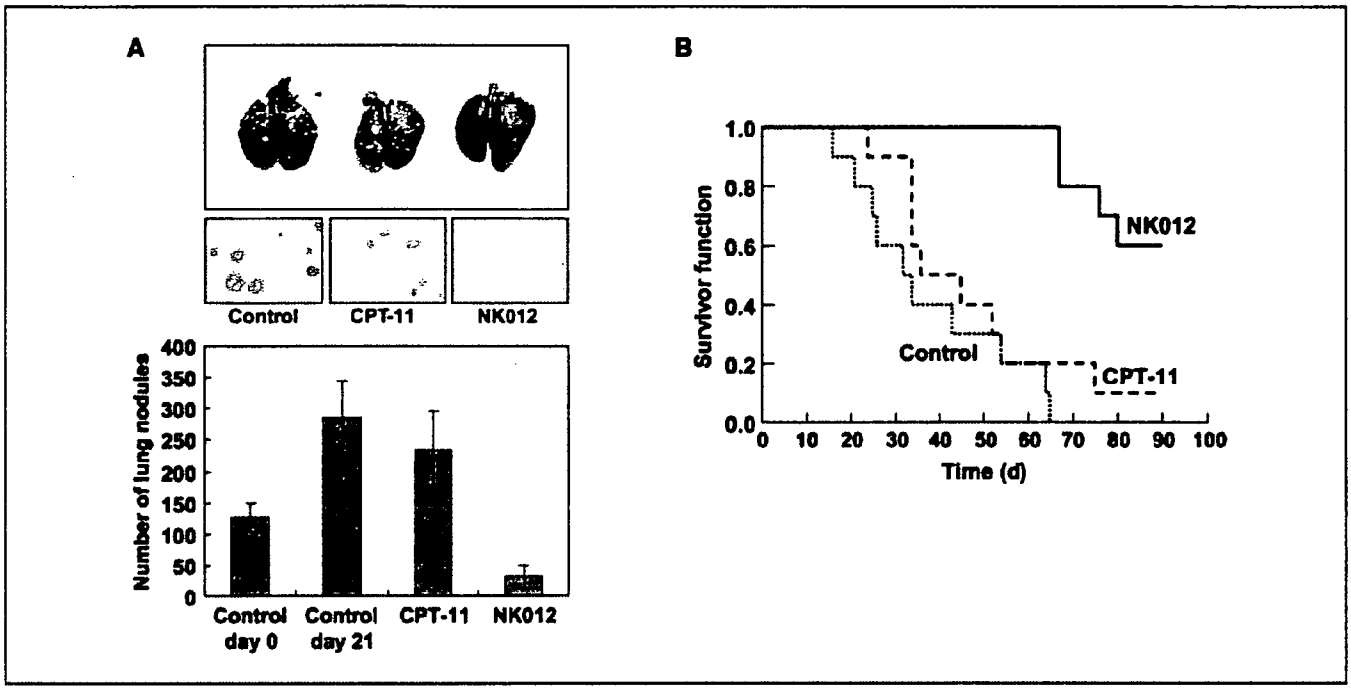

Figure 4. Treatment effect of NK012 on established pulmonary metastasis and survival. NK012 (20 mg/kg/d) and CPT-11 (30 mg/kg/d) were given i.v. to mice with established pulmonary metastasis on days 0 (7 d after Renca inoculation), 4, and 8. *A*, gross and histologic appearances of pulmonary metastases at day 21 (*top*). The metastatic nodules in each mouse were counted. Each group consisted of five mice. *B*, mice were maintained for 90 d after each treatment and survival was assessed by a Kaplan-Meier analysis. Each group consisted of five mice. Experiments were repeated twice with similar results.

the control group ($P < 0.001$), but no significant survival benefit was obtained in CPT-11 treatment group ($P = 0.239$; Fig. 4*B*). Although no severe toxic effects were observed in any mouse treated with NK012, 3 of 10 mice treated with NK012 were sacrificed during the observation period according to the 'Guidelines for Animal Experiments because their body weights had become 10% lower than those of the other mice. However, the sacrificed mice were a little bit smaller than others when they started treatment, and they showed no disseminated lung metastasis (data not shown).

Our results presented here strongly support recent findings reported by us that the macromolecular drug distribution throughout the tumor site was enhanced by the hypervascularity and hyperpermeability, and subsequently higher antitumor activity was achieved (6). We assume that conventional low molecular size anticancer agents almost disappear from the bloodstream without being subjected to the EPR effect before they can reach the target organs (solid tumor). The clinical importance of angiogenesis in human tumors has been shown in several reports indicating a positive relationship between the blood vessel density in the tumor mass and poor prognosis with chemoresistance in patients with various cancers (7–9). Furthermore, recent reports showing that anticancer agents were less active against VEGF-overexpressing tumors (10, 11) may support the idea that low-molecular drugs are not so effective in the treatment of solid tumors which are rich in blood vessels.

Our study thus far has several limitations about clarifying whether extensive angiogenesis in the tumor is an essential determinant for the susceptibility to NK012. In our ongoing study, we found that NK012 also has a striking antitumor activity against some hypovascular tumor models of human pancreatic cancer xenografts.[5] It also remains unclear whether NK012 possesses strong antitumor activity in other metastatic sites besides the lung. It is known that the EPR effect is affected by various permeability factors, such as bradykinin (12), nitric oxide (13). and various cytokines independent of VEGF and hypervascularity (14). Among solid tumors with rapid progression potential, irregularity occurs not only in blood flow and vascular density, but also in the vascular network and anatomic architecture (15, 16), suggesting that EPR effect may be predominantly promoted in rapid-progressive tumor phenotypes and influenced by organ-specific tumor microenvironment. Hoffman and coworkers (17, 18) have developed a technique of surgical orthotopic implantation (SOI) with more clinical features of systemic and aggressive metastases than our conventional animal models. Further preclinical studies using such models as SOI might clarify cancer phenotypes and metastatic organs to which we can apply NK012 more precisely.

The results of chemotherapy in RCCs have been disappointing, as indicated by the low response proportions. However, clinical trials using gemcitabine-containing regimens have been encouraging, with major responses occurring in 5% to 17% of patients (19, 20), suggesting the possibility that chemotherapy is promising as a modality for RCC therapy if anticancer agents can be selectively delivered, released, and maintained around tumor tissues. Our current report highlights the advantages of polymeric micelle-based drug carriers like NK012 as promising modalities for treatment, rather than prevention, of disseminated RCCs with abnormal vascular architecture. The results of our ongoing phase-I

[5] Y. Saito, M. Yasumaga, J. Kuroda, Y. Koga, and Y. Matsumura. Unpublished data.

clinical trial and future phase-II trials of NK012 in patients with advanced solid tumors including RCC might meet or even exceed our expectations.

Acknowledgments

Received 12/10/2007; revised 1/25/2008; accepted 1/31/2008.

Grant support: Grant-in-aid from 3rd Term Comprehensive Control Research for Cancer, Ministry of Health, Labor and Welfare (Y. Matsumura) and Scientific Research on Priority Areas from the Ministry of Education, Culture, Sports, Science and Technology (Y. Matsumura).

The costs of publication of this article were defrayed in part by the payment of page charges. This article must therefore be hereby marked *advertisement* in accordance with 18 U.S.C. Section 1734 solely to indicate this fact.

We thank H. Miyatake and N. Mie for their technical assistance and K. Shiina for her secretarial assistance.

References

1. Matsumura Y, Maeda H. A new concept for macromolecular therapeutics in cancer chemotherapy: mechanism of tumoritropic accumulation of proteins and the antitumor agent smancs. Cancer Res 1986;46:6387–92.
2. Yokoyama M, Miyauchi M, Yamada N, et al. Characterization and anticancer activity of the micelle-forming polymeric anticancer drug adriamycin-conjugated poly(ethylene glycol)-poly(aspartic acid) block copolymer. Cancer Res 1990;50:1693–700.
3. Kataoka K, Harada A, Nagasaki Y. Block copolymer micelles for drug delivery: design, characterization and biological significance. Adv Drug Deliv Rev 2001;47:113–31.
4. Matsumura Y, Hamaguchi T, Ura T, et al. Phase I clinical trial and pharmacokinetic evaluation of NK911, a micelle-encapsulated doxorubicin. Br J Cancer 2004;91:1775–81.
5. Hamaguchi T, Kato K, Yasui H, et al. A phase I and pharmacokinetic study of NK105, a paclitaxel-incorporating micellar nanoparticle formulation. Br J Cancer 2007;97:170–6.
6. Koizumi F, Kitagawa M, Negishi T, et al. Novel SN-38-incorporating polymeric micelles, NK012, eradicate vascular endothelial growth factor-secreting bulky tumors. Cancer Res 2006;66:10048–56.
7. Gasparini G, Harris AL. Clinical importance of the determination of tumor angiogenesis in breast carcinoma: much more than a new prognostic tool. J Clin Oncol 1995;13:765–82.
8. Takahashi Y, Kitadai Y, Bucana CD, Cleary KR, Ellis LM. Expression of vascular endothelial growth factor and its receptor, KDR, correlates with vascularity, metastasis, and proliferation of human colon cancer. Cancer Res 1995;55:3964–8.
9. Williams JK, Carlson GW, Cohen C, Derose PB, Hunter S, Jurkiewicz MJ. Tumor angiogenesis as a prognostic factor in oral cavity tumors. Am J Surg 1994;168:373–80.
10. Natsume T, Watanabe J, Koh Y, et al. Antitumor activity of TZT-1027 (Soblidotin) against vascular endothelial growth factor-secreting human lung cancer *in vivo*. Cancer Sci 2003;94:826–33.
11. Zhang L, Hannay JA, Liu J, et al. Vascular endothelial growth factor overexpression by soft tissue sarcoma cells: implications for tumor growth, metastasis, and chemoresistance. Cancer Res 2006;66:8770–8.
12. Matsumura Y, Maruo K, Kimura M, Yamamoto T, Konno T, Maeda H. Kinin-generating cascade in advanced cancer patients and *in vitro* study. Jpn J Cancer Res 1991;82:732–41.
13. Wu J, Akaike T, Hayashida K, et al. Identification of bradykinin receptors in clinical cancer specimens and murine tumor tissues. Int J Cancer 2002;98:29–35.
14. Maeda H, Fang J, Inutsuka T, Kitamoto Y. Vascular permeability enhancement in solid tumor: various factors, mechanisms involved and its implications. Int Immunopharmacol 2003;3:319–28.
15. Suzuki M, Takahashi T, Sato T. Medial regression and its functional significance in tumor-supplying host arteries. A morphometric study of hepatic arteries in human livers with hepatocellular carcinoma. Cancer 1987;59:444–50.
16. Skinner SA, Tutton PJ, O'Brien PE. Microvascular architecture of experimental colon tumors in the rat. Cancer Res 1990;50:2411–7.
17. An Z, Jiang P, Wang X, Moossa AR, Hoffman RM. Development of a high metastatic orthotopic model of human renal cell carcinoma in nude mice: benefits of fragment implantation compared to cell-suspension injection. Clin Exp Metastasis 1999;17:265–70.
18. Hoffman RM. Orthotopic metastatic mouse models for anticancer drug discovery and evaluation: a bridge to the clinic. Invest New Drugs 1999;17:343–59.
19. Rini BI, Vogelzang NJ, Dumas MC, Wade JL III, Taber DA, Stadler WM. Phase II trial of weekly intravenous gemcitabine with continuous infusion fluorouracil in patients with metastatic renal cell cancer. J Clin Oncol 2000;18:2419–26.
20. Nanus DM, Garino A, Milowsky MI, Larkin M, Dutcher JP. Active chemotherapy for sarcomatoid and rapidly progressing renal cell carcinoma. Cancer 2004;101:1545–51.

Available online at www.sciencedirect.com
ScienceDirect
Biochemical and Biophysical Research Communications 365 (2008) 75–81
BBRC
www.elsevier.com/locate/ybbrc

Yin Yang 1 induces transcriptional activity of p73 through cooperation with E2F1

Shourong Wu [a,c], Saomi Murai [a], Kazunori Kataoka [b,c], Makoto Miyagishi [d,*]

[a] Department of Chemistry and Biotechnology, Graduate School of Engineering, The University of Tokyo, 7-3-1 Hongo, Bunkyo-ku, Tokyo 113-8656, Japan
[b] Department of Materials Engineering, Graduate School of Engineering, The University of Tokyo, 7-3-1 Hongo, Bunkyo-ku, Tokyo 113-8656, Japan
[c] Division of Clinical Biotechnology, Center for Disease Biology and Integrative Medicine, The University of Tokyo, 7-3-1 Hongo, Bunkyo-ku, Tokyo 113-0033, Japan
[d] 21st Century COE Program, Graduate School of Medicine, The University of Tokyo, 7-3-1 Hongo, Bunkyo-ku, Tokyo 113-0033, Japan

Received 18 October 2007
Available online 1 November 2007

Abstract

The transcription factor p73 is a structural homologue of p53 and plays an important role in tumorigenesis, differentiation and development. However, the regulation of p73 pathway has not been wholly understood. Here we reported that YY1-silencing resulted in significant reductions in the activities of the p73 promoters and the endogenous p73 expression level, conversely, overexpression of YY1 could induce the activities of them. Furthermore, we showed that YY1 and E2F1 have synergistic effect on p73 promoter activity. The results of YY1-silencing and E2F1-silencing alone revealed that both factors are involved in the doxorubicin-induced activation of p73 promoter. Immunofluorescence staining and co-immunoprecipitation assays demonstrated that cooperation of YY1 and E2F1 is concomitant with physical interaction in nuclei. The results presented here suggested the cooperative transcriptional regulation of p73 by YY1 and E2F1, and might provide a new regulation mechanism by the YY1 network on tumorigenesis, differentiation and development.

Keywords: Yin Yang 1; E2F1; p73; Transcriptional activation; Synergistic effect

Yin Yang 1 (YY1) is a multifunctional transcription factor that exerts its effects on genes involved in various biological processes via its ability to initiate, activate, or repress transcription depending upon the context to which it binds, directly or indirectly via cofactor recruitments [1–3]. Today, YY1 is known to have a fundamental role in normal biological processes such as embryogenesis, differentiation, DNA replication, and cellular proliferation [3]. YY1-deficient embryos died at the time of implantation, and furthermore, its heterozygote knockout mice displayed significant growth retardation and neurological defects, indicating that YY1 plays an indispensable role in embryonic development and neuronal differentiation [4,5]. Recently, the physiologic significance of YY1 activity has also been reported to be associated with tumor biology [3,5,6]. It was known that YY1 is overexpressed in prostate cancer and sarcoma. Therefore, it is helpful to explain the cancer biological function of YY1 via studying its putative interactions with cell cycle regulators, death genes, as well as transcription factors and cofactors in the suppression or progression of various malignancies.

P73 has initially been known as a homologue of p53. They share relatively high sequence homology that includes an N-terminal transactivating (TA) domain and a central DNA binding domain. P73 has been reported to induce cell growth arrest and apoptosis in some cell lines irrespective of p53 status [7,8], and activate some p53 responsive genes, such as bax, cyclin G, IGF-BP3, and 14-3-3σ [9]. However, despite these similarities, p53 and p73 also show some fundamental differences in mechanisms and responses to DNA damage, and furthermore, in the phenotypes of their knockout mice. P73-null mice showed some defects in nervous system, which is not exhibited in p53-null mice

* Corresponding author. Fax: +81 3 5628 3770.
E-mail address: makoto-m@umin.ac.jp (M. Miyagishi).

0006-291X/$ - see front matter © 2007 Elsevier Inc. All rights reserved.
doi:10.1016/j.bbrc.2007.10.145

[10,11]. On the other hand, p73-null mice do not develop spontaneous tumor formation while p53 knockout mice exhibit high susceptibility to tumorigenesis [3]. Furthermore, a very recent report showed that p73 could promote cell growth in a synergistic manner with the proto-oncogene c-Jun, and conversely, silencing p73 resulted in the reduction of growth rate and decrease of cyclin D1, indicating that p73 could act positively in tumorigenesis [12]. Therefore, p73 has a complex functions in biological processes including apoptosis, differentiation, tumorigenesis, and cell growth.

E2F1 has been identified as a regulation factor for p73 transcription. Pediconi et al. reported that responding to certain DNA damages, E2F1, but not E2F2, E2F3, or E2F4, can recruit the p73 promoter and efficiently and specifically activate its transactivation [13]. However, transcriptional regulation factors of the p73 promoter, excepting E2F1, remain unknown. Identification of other regulators that might control p73 is needed to further understand its functions and roles in tumorigenesis, differentiation and development.

Here, we identified a transcription factor, YY1, as a novel regulator of p73 transcription. Moreover, we showed that YY1 cooperates with E2F1 to induce the transcriptional activity of p73. Taken together, these findings not only shed new light on the nature of YY1's biological activities but also indicate the complex regulation mechanism of p73 in diverse biological processes.

Materials and methods

Cell cultures and chemicals. The U2OS, and HCT116 cells were obtained from the American Type Culture Collection; the SaOS2 cells were from Riken Cell Bank (Tsukuba, Japan). The U2OS and HEK293T cells were maintained in Dulbecco's modified Eagle's medium (Sigma–Aldrich) containing 10% fetal bovine serum (FBS, Invitrogen); The HCT116 and SaOS2 cells were maintained in McCoy's 5A medium (Invitrogen) containing 10% FBS or 15% FBS, respectively.

Plasmids and constructs. The long human p73-Luciferase reporter, which contains the p73 gene fragment −4052 to +438, was generously provided by Prof. Levrero (University of Rome 'La Sapienza', Rome, Italy) [13]. The short human p73-Luciferase reporter (−857 to +71) and the human p21-Luciferase reporter were constructed by inserting each PCR products into the BglII site and HindIII site of the pGL4 basic vector (Promega).

To generate the Flag-E2F1 expression vector, pcEF9-Flag-E2F1, the coding regions of human E2F1 were amplified by PCR and inserted into the HindIII and BamHI restriction sites of pcEF9 vector [14]. For the YY1 expression vector, the coding region of human YY1 was inserted into the pcDNA3 vector (Invitrogen). For construction of the HA-YY1 vector for use in immunofluorescence staining, the YY1 coding region in pcDNA3-YY1 was excised and inserted into the BamHI and EcoRI sites of pcDNA3-HA. To construct the Flag-YY1 expression vector for use in co-immunoprecipitation experiments, the Flag-YY1 coding region fragment was generated by PCR using pcDNA3-YY1 as a template, and the PCR product was again inserted into pcDNA3 vector predigested with BamHI and EcoRI.

RNA interference. To construct siRNA expression vectors, oligonucleotides with a hairpin, overhanging sequences and terminator were synthesized, annealed and then inserted into the BspMI sites of the pcENTRhU6 vector [15]. Based on the results of applying our algorithm [16], we identified the target sequences for YY1 and E2F1 genes: siYY1-1 (GCAAGAAGAGTTACCTCAG), siYY1-2 (GGCAGAATTTGCTAGAATG), siE2F1 (GGCTGGACCTGGAAACTGA). We used a T7 siRNA expression vector, which contains a stretch of 7 thymine (Ts) terminator sequences exactly downstream of the U6 promoter, as a control.

Transient transfection and luciferase assays. The U2OS and HCT116 cells were transfected with the different p73 firefly luciferase reporters along with indicated amounts of expression vectors and *Renilla* luciferase expression vector (pRL-SV40, Promega) for transfection normalization. For knockdown experiments, HCT116 and U2OS were transfected with siRNA expression vectors, and 24 h later selection was performed by puromycin. The selected cells were transfected with p73-luciferase reporters and pRL-SV40. FuGENE6 (Roche) were used for all transfections in U2OS cells, and Lipofectamine™ 2000 (Invitrogen) for HCT116 cells. Forty-eight hours after transfection, luciferase assays were performed in triplicate using the Dual Luciferase Assay System (Promega). All relative luciferase activities were determined by calculating the ratio between firefly and *Renilla* luciferase activities, and the results were shown as means ± SDs.

Real-time RT-PCR analysis. The total RNA was isolated using TRIZOL® Reagent (Invitrogen) and treated with DNase I (Qiagen) according to the manufacturer's instructions. The total RNA (1 μg) were then reverse-transcribed using a QuantiTect Reverse Transcription Kit (Qiagen). Real-time PCR was carried out using an Applied Biosystems 7500 system (Applied Biosystems) and QuantiTect® SYBR Green PCR Master Mix (Qiagen). All reactions were run in triplicate and expressional results were normalized to actin. Data were expressed as means ± SDs of triplicate wells. The primer sequences are available upon request.

Western blotting analysis. The cells were lysed in whole-cell extract buffer (50 mM Tris–HCl, pH 7.3, 10% glycerol, 250 mM sodium chloride, 2 mM EDTA, 0.1% Nonidet P-40, and 1 mM NaF) with protease inhibitors (complete cocktail; Roche), and the lysate samples proteins were electrophorated on 10% SDS–polyacrylamide gel and transferred to a polyvinylidene fluoride (PVDF) membrane (Millipore). After blocking, the membrane was incubated with indicated primary antibodies, and then with horseradish peroxidase (HRP)-conjugated secondary antibody IgG (Amersham Biosciences). Detections were performed with ECL Plus™ reagent (Amersham Biosciences). Antibodies used for western blotting were a rabbit polyclonal anti-E2F1 antibody (C-20, Santa Cruz), a mouse monoclonal anti-YY1 antibody (H-10, Santa Cruz), and a rabbit monoclonal anti-actin antibody (Sigma–Aldrich).

Immunofluorescence staining. The U2OS cells were seeded on cover-slips in 6-well plates and transfected with plasmids encoding HA-YY1 and E2F1. Forty-eight hours after transfection, cells were fixed for 20 min at room temperature with 10x PBS containing 4% paraformaldehyde, and permeabilized for 30 min in PBS containing 0.1% Triton X-100. After blocking, cover-slips were incubated at room temperature for 1 h in a 1:250 dilution of rat anti-HA and a 1:50 dilution of rabbit anti-E2F1 (Santa Cruz). Slides were then incubated for 1 h with a 1/1000 dilution of Alexa Fluor® 488 goat anti-rat IgG (H + L) and a 1/1000 dilution of Alexa Fluor® 568 goat anti-rabbit IgG (H + L) (Molecular Probes).

Co-immunoprecipitation. HEK293T cells were transfected with 10 μg of pcDNA3-Flag-YY1 or pcDNA3 using Lipofectamine™ 2000. Transfected cells were harvested 48 h post-transfection for Immunoprecipitation–Western blotting. Cell lysates were solved in lysis buffer (10 mM HEPES, pH 7.5, 100 mM KCl, 0.1% NP-40) with protease inhibitors on ice for 30 min and then cleared by centrifugation at 15,000 rpm. The supernatants were incubated at 4°C for 1 h with protein G-beads in the presence of 3 μg of anti-flag monoclonal antibody. Then, the immunoprecipitated proteins were subjected to western blot analysis using anti-E2F1 antibody as described above.

Results and discussion

YY1-silencing reduces the transcriptional activity of p73

Although YY1 is well known as a p53 inhibitor, recent reports have implied that YY1 has p53-independent

pathway(s) for cell cycle regulation and apoptosis [5,6]. To elucidate novel pathways of YY1, we generated siRNA vectors, siYY1-1 and siYY1-2, targeted against two different sites of YY1 for knock-down experiments. The two siRNA vectors were used to ensure elimination of off-target effect of RNAi. Western blot analysis of YY1 siRNA vectors-transfected cells revealed that both siYY1-1 and siYY1-2 could significantly suppress the endogenous level of YY1 without affecting levels of E2F1 (Fig. 1A). Furthermore, using a p21 promoter/reporter construct, which is essentially dependent on p53, we confirmed the ability of the siYY1 vectors to functionally repress endogenous YY1, which resulted in the up-regulation of p53, and subsequently, the increase of p21 promoter/reporter activities (Supplemental Fig. 1). Thus, the siRNA vectors for YY1 used here were able to knockdown and block the endogenous function of YY1 effectively and specifically.

Next, using a p73 promoter/reporter construct, we found that in contrast to the case of the p21 promoter, YY1-silencing led to a significant reduction of p73 promoter activity in both HCT116 cells and U2OS (Fig. 1B and 1C). To further confirm this finding, we performed real-time RT-PCR using total RNA extracted from YY1-silenced U2OS cells. The results showed that the reduction of p73 mRNA level was observed in the YY1-silenced U2OS cells (Fig. 1D), indicating that in contrast with p53, knockdown of YY1 was able to reduce the transcriptional activity of p73. The results implied the novel regulation of p73 by YY1.

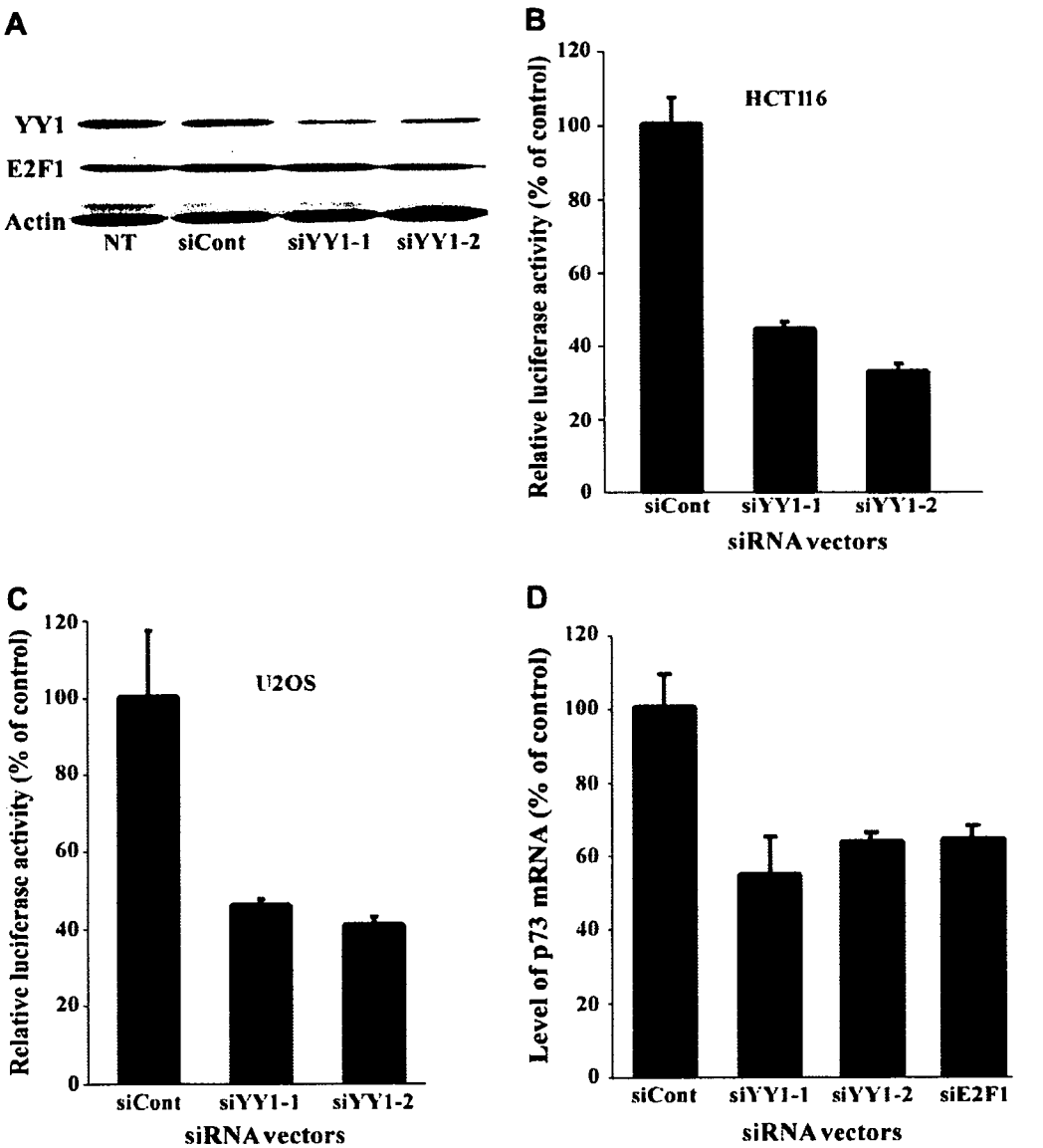

Fig. 1. The knockdown of YY1 reduces the transcriptional activity of p73. (A) HCT116 cells were transfected with siYY1-1 or siYY1-2 vectors or the siCont vector, the Western blotting was performed for detection of YY1 and E2F1. NT: non-transfected cells. (B–C) The effect of YY1-silencing on p73 promoter-driven transcription in HCT116 cells and U2OS cells. The indicated siRNA vectors-transfected HCT116 cells (B) and U2OS cells (C) were co-transfected with p73 luciferase (−4052/+438)/reporter and *Renilla* luciferase expression vector (pRL-SV40). Dual luciferase activity assay was performed 48 h after transfection. (D) Expression of p73 mRNA in YY1, E2F1-knocked down U2OS cells, determined by real-time RT-PCR analysis.

Effect of YY1 and E2F1 overexpression on the transcription activity of p73

Next, to assess the effect of YY1 overexpression and to confirm that of E2F1, a well-known p73 regulator, on p73 promoter activity, we generated a YY1-expression vector (pcDNA3-YY1) and an E2F1 expression vector (pcEF9-Flag-E2F1), and confirmed their expressions by Western blot analysis (Fig. 2A). Furthermore, the p53-inhibition activity of exogenous YY1 was also confirmed by p21 luciferase/reporter (Supplemental Fig. 2). Then, a different dose of the pcDNA3-YY1 was co-transfected into U2OS cells together with the two p73 reporters (Fig. 2B). The results were in agreement with those of knockdown experiments, as overexpression of YY1 led to the activation of the p73 promoter in a plasmid-dose dependent manner. Similar results were also obtained from SaOS2 cells, a p53 deficient human osteocarcinoma cell line (Fig. 2C), indicating that the YY1-induced p73 transcriptional activity is independent on p53 status. On the other hand, overexpressing E2F1 by co-transfecting E2F1 expression vector with the p73 promoter (−4052/+438)/reporter (Fig. 2D) or the p73 promoter (−857/+71)/reporter (Supplemental Fig. 3) resulted in the significant induction of both p73 reporters' activities, as shown previously [13]. Moreover, YY1 overexpression in U2OS cells resulted in the increase of endogenous p73 mRNA (Fig. 2E), similar with the effect of doxorubicin (Fig. 2F), which has been known to induce p73 activity via E2F1.

Collectively, the results from the knockdown and overexpression experiments for YY1 clearly identified the previously unsuspected role of YY1, i.e., the possibility that tumor activator gene YY1 up-regulates the transcriptional activity of p73. Recently, other evidences showed that spontaneous tumor formation did not develop in p73-null mice, and infrequent p73 mutations or overexpression of p73 protein was seen in a variety of tumors [17]; raising

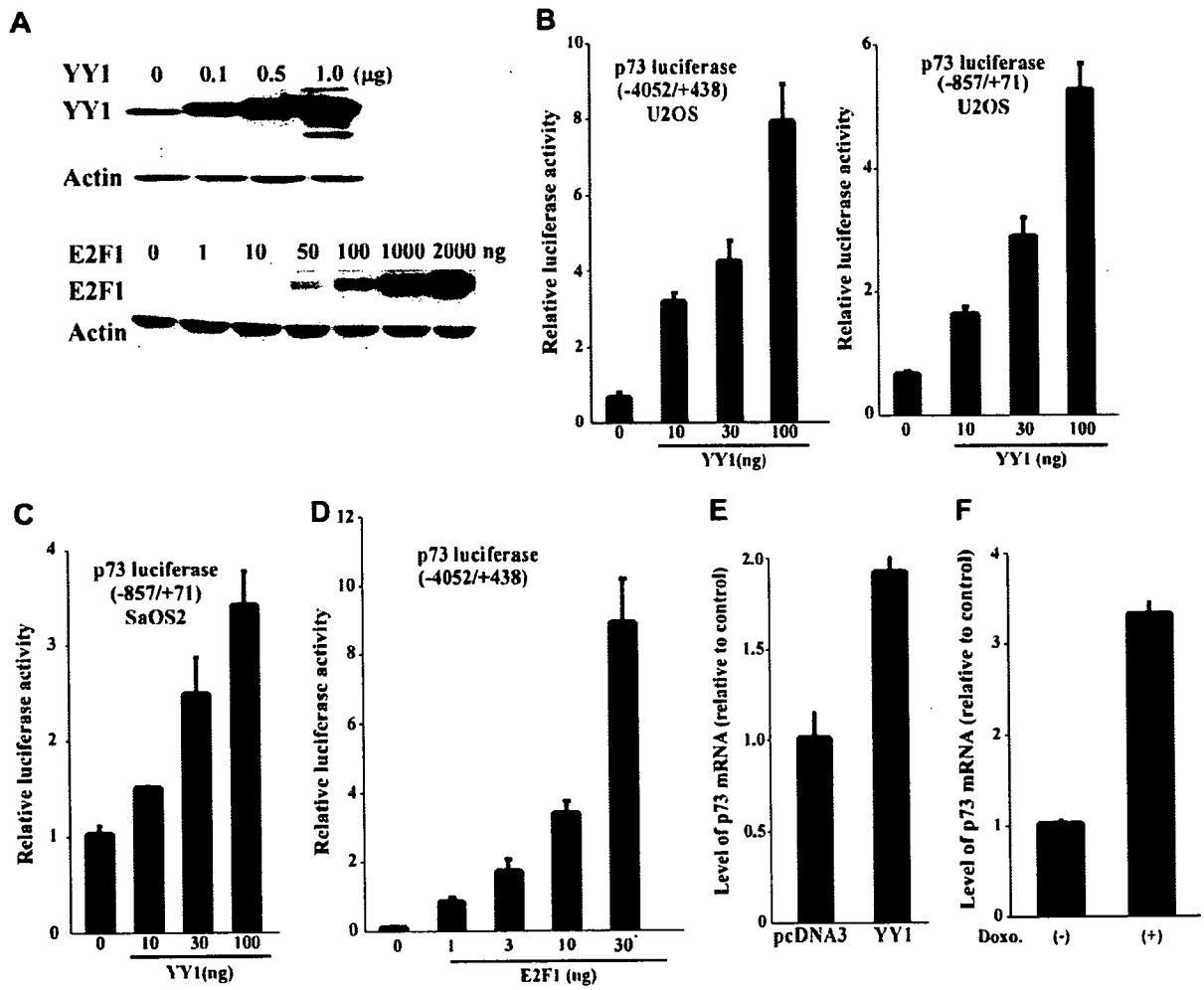

Fig. 2. The induction of p73 promoter activity by YY1 and E2F1. (A) Western blotting analysis of YY1 (upper panel) and E2F1 (lower panel) in HCT116 cells transfected with pcDNA3-YY1 or pcEF9-Flag-E2F1. (B) The effect of YY1 on the activities of p73 luciferase (−4052/+438)/reporter (left) or p73 luciferase (−857/+71)/reporter (right) in U2OS cells, determined by dual luciferase assay 48 h after transfection. (C) The effect of YY1 on the activities of p73 luciferase (−857/+71)/reporter in SaOS2 cells. (D) The effect of E2F1 on the activities of the p73 luciferase (−4052/+438)/reporter in HCT116 cells. (E) Expression of p73 mRNA in U2OS cells transfected with pcDNA3-YY1, determined by real-time RT-PCR analysis 12 h after transfection. (F) Expression of p73 mRNA in U2OS cells treated with doxorubicin (2 μM), determined by real-time RT-PCR analysis 24 h after treatment.

the question of the function of p73 as a tumor suppressor gene. A very recent work by Vikhanskaya et al. provided a potential answer to this question [12]. They found that p73 could promote cellular growth in a synergistic manner with the proto-oncogene c-Jun through AP-1 up-regulation, thus, p73 could positively act for tumorigenesis. Our results were consistent with their results. Moreover, it has also been reported that Yin Yang 1 is essential for oligodendrocyte progenitor differentiation and B-cell development [18,19]. Thus, our findings might also provide an important clue for unveiling molecular functions and mechanisms of YY1 and p73 pathway in neural differentiation and development. Therefore, we next addressed how YY1 regulates p73 gene transcription, specifically, whether there is a relationship between YY1 and E2F1 in regulating the transcriptional activity of p73.

The synergistic effect of YY1 and E2F1 on p73 transactivation

To examine whether there is cooperative regulation of p73 promoter activity by E2F1 and YY1, we performed co-transfection experiments using the p73 promoter (−4052/+438)/reporter, pcDNA3-YY1 and pEF9-E2F1 vectors. The U2OS cells co-transfected with both E2F1-expression and YY1-expression vectors showed a signification enhancement in the activity of p73 promoter compared to cells transfected with either of the vectors alone (Fig. 3A). Furthermore, in experiments with serial doses of YY1-expression vector under the constant presence of pEF9-E2F1, we found that in the presence of E2F1, the activity of p73 promoter increased in a dose-dependent manner with increasing amount of pcDNA-YY1 vector (Fig. 3B). These results demonstrated that YY1 could induce the transcriptional activity of p73 in a synergistic fashion with E2F1.

Previously, Schlisio et al. reported that E2F2 and E2F3, the members of E2F family, could interact with YY1 through mediation of the RYBP protein on the cdc6 promoter; they suggested that the interaction of E2Fs family with YY1 might determine the specificity of E2F2/E2F3 or E2F1 for different promoters [20]. In this study, we observed considerable cooperative transcriptional activation between E2F1 and YY1 on the p73 promoter. However, this functional interaction between YY1 and E2F1 might be not general, as the overexpression of YY1 did not show any significant activation of other well-defined E2F1-dependent promoters tested (DNMT1 and DHFR, data not shown), suggesting that the promoter specificity of E2F1 and E2F2/E2F3 is not simply determined by the

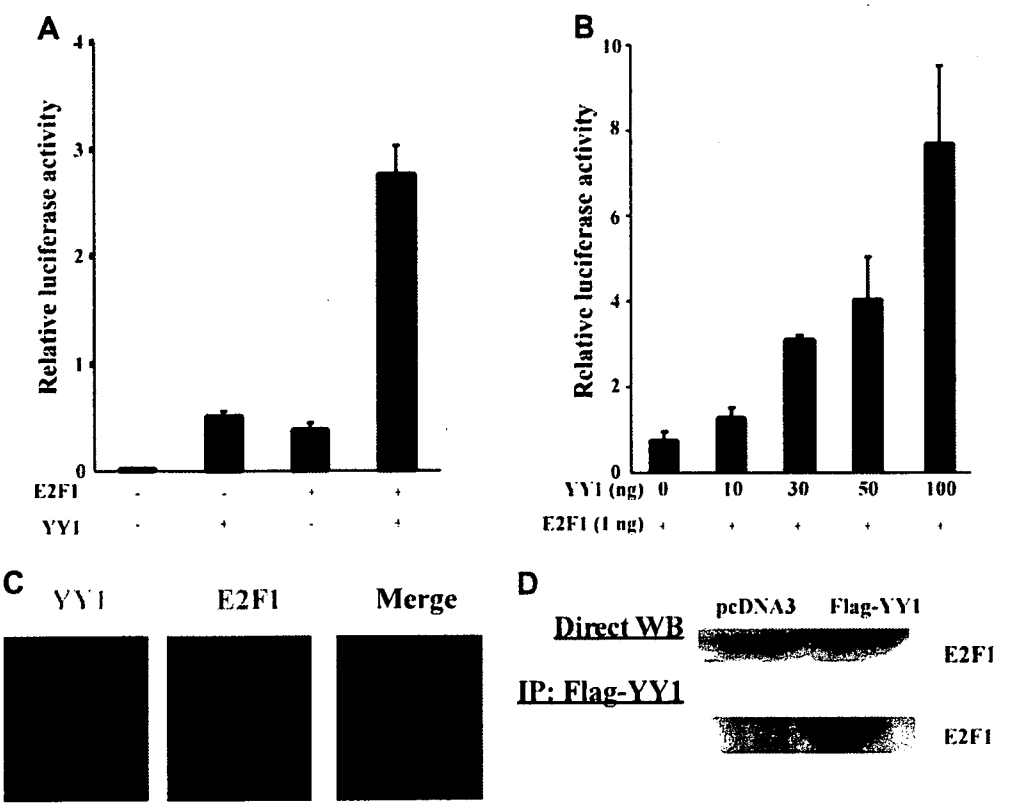

Fig. 3. The synergistic effect of YY1 and E2F1 on the transcriptional activation p73. (A) The activity of p73 luciferase (−4052/+438)/reporter in U2OS cells transfected with mock vector, pcDNA3-Flag-YY1 (50 ng), pcEF9-Flag-E2F1 (1 ng), or both pcDNA3-YY1 (50 ng) and pcEF9-Flag-E2F1 (1 ng). Dual luciferase assay was performed 48 h after transfection. (B) The activity of p73 luciferase (−4052/+438)/reporter in U2OS cells transfected with the indicated amounts of pcDNA3-YY1 and the constant amount of pcEF9-Flag-E2F1 (1 ng). (C) Immunofluorescence staining of YY1 and E2F1 in U2OS cells. (D) Co-immunoprecipitation of E2F1 and YY1 in HEK293T cells. Cells were lysed and pulled-down with anti-Flag antibody.

interaction with YY1, but might be determined by other undefined factors interacting with E2Fs and/or the epigenetic status of the promoters.

Co-localization and interaction between YY1 and E2F1

To understand the cellular and molecular mechanisms of the synergistic effects between YY1 and E2F1 on p73 promoter activation, we first examined the subcellular localization of YY1 and E2F1. As shown in Fig. 3C, YY1 was largely colocalized with E2F1 in the nucleus. Next, we examined the physical interactions between YY1 and E2F1 by performing co-immunoprecipitation experiments. The results showed that E2F1 immunoprecipitated in cells transfected with the Flag-YY1-expression vector, whereas no band was detected in cells transfected with the control vector (Fig. 3D). These observations demonstrated the direct physical association between YY1 and E2F1.

Role of YY1 in DNA damage-induced transcriptional activity of p73 promoter

As reported previously, the p73 promoter was activated E2F1-dependently by doxorubicin, a DNA damaging agent [13]. Therefore, we examined whether YY1 contributed to doxorubicin-induced p73 transcriptional activation. YY1-silenced cells showed significant reduction in the activation of the p73 promoter induced by doxorubicin (Fig. 4A, B), which was similar to that of E2F1-silencing cells.

Furthermore, p73 promoter activation by doxorubicin treatment has been reported to be critically dependent on

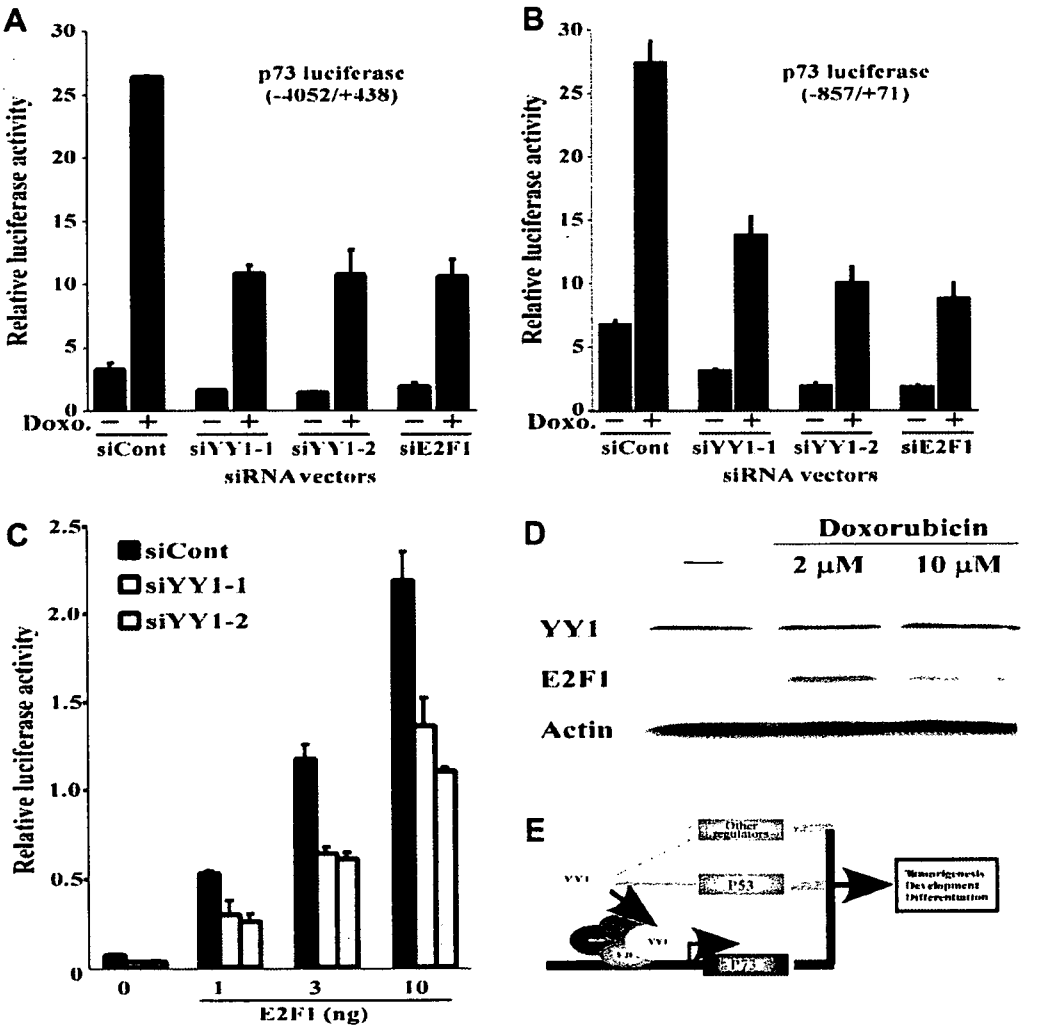

Fig. 4. Involvement of YY1 in transcriptional activation of p73 induced by doxorubicin. (A, B) The activity of p73 promoter in the YY1-silenced U2OS cells under doxorubicin treatment. siYY1-1, siYY1-2 or siE2F1 vectors-transfected U2OS cells were co-transfected with p73 luciferase (−4052/+438)/reporter (A) or (−857/+71)/reporter (B) and pRL-SV40. Twenty-four hours after transfection, U2OS cells were untreated or treated with doxorubicin (2 μM), and 24 h later, dual luciferase assay was performed. (C) The effect of YY1-silencing on p73 promoter activity induced by E2F1 in U2OS cells. The indicated siRNA vectors-transfected U2OS cells were co-transfected with p73 luciferase (−4052/+438)/reporter and increasing amount of pcEF9-Flag-E2F1. (D) Western blot analysis of E2F1 and YY1 in HCT116 cells treated by doxorubicin. (E) A model of the co-regulation of YY1 and E2F1 on p73.

E2F1 [13]. Based on the interaction of E2F1 and YY1, we next tested whether p73 promoter activation by E2F1 overexpression also showed the YY1 dependency. The YY1-knocked down cells were co-transfected with serial doses of E2F1-expression vectors and the p73 reporter vector. As shown in Fig. 4C, in YY1-silenced cells, the p73 promoter activation induced by E2F1 was significantly reduced, which was a comparable suppressive effect as that of doxorubicin-treated cells, suggesting that the YY1 signal might be constitutive during doxorubicin treatment. Together with the results of Western blot analysis (Fig. 4D), which revealed that only endogenous E2F1, not YY1 expression was induced by doxorubicin treatment, these data indicated that cooperative action between the constitutive YY1 and the inducible E2F1 contributes to the activation of the p73 promoter under the treatment with doxorubicin. Furthermore, YY1-silencing did not affect the expression of endogenous E2F1 (Fig. 1A), which also strongly suggested that YY1 induces the transcriptional activity of p73 by cooperation with E2F1, not via increasing E2F1.

Taken together, our results uncovered a novel function of YY1 on E2F1-mediated p73 regulation. We summarized the model in Fig. 4E. The fact that YY1 affects p53 family members opened up an attractive possibility that needs further investigation, that is, YY1 might function as a key integrator or modulator of various pathways in the network that includes p53 family members and regulators concerned with cancer progression, development and differentiation.

Acknowledgments

We thank Prof. Massimo Levrero at the University of Rome 'La Sapienza' for kindly providing the p73 reporter vector. This work was partially supported by a grant from the 21st Century COE Program, School of Medicine, The University of Tokyo, and a grant for Research on Psychiatric and Neurological Diseases and Mental Health, the Ministry of Health, Labour and Welfare of Japan.

Appendix A. Supplementary data

Supplementary data associated with this article can be found, in the online version, at doi:10.1016/j.bbrc.2007.10.145.

References

[1] Y. Shi, E. Seto, L.S. Chang, T. Shenk, Transcriptional repression by YY1, a human GLI-Kruppel-related protein, and relief of repression by adenovirus E1A protein, Cell 67 (1991) 377–388.
[2] K. Park, M.L. Atchison, Isolation of a candidate repressor/activator, NF-E1 (YY-1, delta), that binds to the immunoglobulin kappa 3' enhancer and the immunoglobulin heavy-chain mu E1 site, Proc. Natl. Acad. Sci. USA 88 (1991) 9804–9808.
[3] S. Gordon, G. Akopyan, H. Garban, B. Bonavida, Transcription factor YY1: structure, function, and therapeutic implications in cancer biology, Oncogene 25 (2006) 1125–1142.
[4] M.E. Donohoe, X. Zhang, L. McGinnis, J. Biggers, E. Li, Y. Shi, Targeted disruption of mouse Yin Yang 1 transcription factor results in peri-implantation lethality, Mol. Cell. Biol. 19 (1999) 7237–7244.
[5] B. Affar el, F. Gay, Y. Shi, H. Liu, M. Huarte, S. Wu, T. Collins, E. Li, Essential dosage-dependent functions of the transcription factor yin yang 1 in late embryonic development and cell cycle progression, Mol. Cell. Biol. 26 (2006) 3565–3581.
[6] G. Sui, B. Affar el, Y. Shi, C. Brignone, N.R. Wall, P. Yin, M. Donohoe, M.P. Luke, D. Calvo, S.R. Grossman, Yin Yang 1 is a negative regulator of p53, Cell 117 (2004) 859–872.
[7] R. Agami, G. Blandino, M. Oren, Y. Shaul, Interaction of c-Abl and p73alpha and their collaboration to induce apoptosis, Nature 399 (1999) 809–813.
[8] C.A. Jost, M.C. Marin, W.G. Kaelin Jr., p73 is a simian [correction of human] p53-related protein that can induce apoptosis, Nature 389 (1997) 191–194.
[9] G. Melino, F. Bernassola, M. Ranalli, K. Yee, W.X. Zong, M. Corazzari, R.A. Knight, D.R. Green, C. Thompson, K.H. Vousden, p73 Induces apoptosis via PUMA transactivation and Bax mitochondrial translocation, J. Biol. Chem. 279 (2004) 8076–8083.
[10] G. Meyer, C.G. Perez-Garcia, H. Abraham, D. Caput, Expression of p73 and Reelin in the developing human cortex, J. Neurosci. 22 (2002) 4973–4986.
[11] T. Ozaki, M. Hosoda, K. Miyazaki, S. Hayashi, K. Watanabe, T. Nakagawa, A. Nakagawara, Functional implication of p73 protein stability in neuronal cell survival and death, Cancer Lett. 228 (2005) 29–35.
[12] F. Vikhanskaya, W.H. Toh, I. Dulloo, Q. Wu, L. Boominathan, H.H. Ng, K.H. Vousden, K. Sabapathy, p73 supports cellular growth through c-Jun-dependent AP-1 transactivation, Nat. Cell Biol. 9 (2007) 698–705.
[13] N. Pediconi, A. Ianari, A. Costanzo, L. Belloni, R. Gallo, L. Cimino, A. Porcellini, I. Screpanti, C. Balsano, E. Alesse, A. Gulino, M. Levrero, Differential regulation of E2F1 apoptotic target genes in response to DNA damage, Nat. Cell Biol. 5 (2003) 552–558.
[14] M. Miyagishi, R. Fujii, M. Hatta, E. Yoshida, N. Araya, A. Nagafuchi, S. Ishihara, T. Nakajima, A. Fukamizu, Regulation of Lef-mediated transcription and p53-dependent pathway by associating beta-catenin with CBP/p300, J. Biol. Chem. 275 (2000) 35170–35175.
[15] M. Miyagishi, K. Taira, U6 promoter-driven siRNAs with four uridine 3' overhangs efficiently suppress targeted gene expression in mammalian cells, Nat. Biotechnol. 20 (2002) 497–500.
[16] M. Miyagishi, K. Taira, Strategies for generation of a siRNA expression library directed against the human genome, Oligonucleotides 13 (2003) 325–333.
[17] F. de Nigris, C. Botti, A. de Chiara, R. Rossiello, G. Apice, F. Fazioli, C. Fiorito, V. Sica, C. Napoli, Expression of transcription factor Yin Yang 1 in human osteosarcomas, Eur. J. Cancer 42 (2006) 2420–2424.
[18] Y. He, J. Dupree, J. Wang, J. Sandoval, J. Li, H. Liu, Y. Shi, K.A. Nave, P. Casaccia-Bonnefil, The transcription factor Yin Yang 1 is essential for oligodendrocyte progenitor differentiation, Neuron 55 (2007) 217–230.
[19] H. Liu, M. Schmidt-Supprian, Y. Shi, E. Hobeika, N. Barteneva, H. Jumaa, R. Pelanda, M. Reth, J. Skok, K. Rajewsky, Yin Yang 1 is a critical regulator of B-cell development, Genes Dev. 21 (2007) 1179–1189.
[20] S. Schlisio, T. Halperin, M. Vidal, J.R. Nevins, Interaction of YY1 with E2Fs, mediated by RYBP, provides a mechanism for specificity of E2F function, EMBO J. 21 (2002) 5775–5786.

Original Article

A Novel Contrast Medium Detects Increased Permeability of Rat Injured Carotid Arteries in Magnetic Resonance T2 Mapping Imaging

Yutaka Imai[1], Eiji Kaneko[1], Tetuichi Asano[1], Michiaki Kumagai[2], Masumi Ai[1], Akio Kawakami[1], Kazunori Kataoka[2], and Kentaro Shimokado[1]

[1]Department of Geriatrics and Vascular Medicine, Tokyo Medical and Dental University Graduate School, Tokyo, Japan.
[2]Department of Materials Science, Graduate School of Engineering, the University of Tokyo, Tokyo, Japan.

Aim: Aim of this study was to directly detect increased permeability of vascular lesions by magnetic resonance imaging.
Methods: A novel contrast medium with a mean hydrodynamic diameter of 100 nm was prepared from monodispersed iron colloids incorporated into micelles of block copolymers composed of polyethylene glycol and polyamino acid. T2 mapping was applied to differentiate the minimal shortening of T2 relaxation time in balloon-injured rat carotid arteries.
Results: The novel contrast medium accumulated in deendothelialized arteries. T2 relaxation times of injured and uninjured arteries were 50.6 ± 9.5 ms and 26.9 ± 2.4 ms, respectively (the mean ± SD, $p < 0.01$, $n = 5$). The novel contrast medium, but not commercially available contrast media, shortened the T2 relaxation time of the injured artery to 35.5 ± 9.7 ms ($p < 0.01$, $n = 4$).
Conclusion: A novel iron contrast medium enhanced the lesions with increased permeability. The contrast medium in combination with T2 mapping may be useful to detect unstable atherosclerotic plaques.

J Atheroscler Thromb, 2007; 14:65-71.

Key words; Contrast media, Drug delivery system, T2 relaxation time, Vasculature

Introduction

Non-invasive assessment of arteriosclerosis is important, and advances in magnetic resonance (MR) imaging have made it possible to obtain high resolution and *in vivo* visualization of atherosclerotic plaque of complex composition[1, 2]. For the practical application of MR imaging in the diagnosis of vascular lesions, improvement of techniques to analyze MR information and the development of contrast media are necessary, along with improvement of equipment that can be used to obtain information quickly[3].

To improve the analysis of MR information, various techniques have been developed, including multiple contrast weighting[4], MR direct thrombus imaging[5] and black-blood technique[6, 7]. T2 mapping is potentially useful for this purpose. By integrating signals of various echo times, T2 mapping can detect small differences in T2 relaxation time. T2 mapping also gives consistent images regardless of magnetic field intensity whereas other techniques that involve the T1 relaxation process are affected by the condition and can give quite different images[8]. Recently, T2 mapping has been used to detect lesions in the brain[9], cartilage[10, 11] and liver[12] of humans and small animals, and was found to sensitively detect small differences of the T2 relaxation time between the lesions and normal tissue; however, T2 mapping has not been applied to vascular MR imaging.

Various contrast media have been developed to detect vascular lesions. Superparamagnetic iron oxide enhanced MR images of atherosclerotic lesions in rabbits[13] and humans[14]. It has been speculated that this contrast medium is phagocytosed by macrophages and accumulates in the lesions. The limitation of this agent

Address for correspondence: Kentaro Shimokado, Department of Geriatrics and Vascular Medicine, Tokyo Medical and Dental University Graduate School, 1-5-45 Yushima, Bunkyo-ku, Tokyo 113-8519, Japan.
E-mail: k.shimoka.vasc@tmd.ac.jp
Received: October 2, 2006
Accepted for publication: November 25, 2006

is that a high dose is necessary to obtain good contrast and accumulation takes time, up to 24 hours. Gadofluorine (Gd) detected macrophage-rich lesions of atherosclerotic plaques[15]. Other Gd-based contrast media have been developed to detect specific components such as platelets, angiogenesis markers and fibrin, and they have been used successfully to characterize plaques[3]. Recently, Evans blue-conjugated Gd was reported to enhance injured arteries[16].

In this study, we aimed to directly detect vascular lesions with increased permeability for macromolecules. We made a novel contrast medium by developing a new iron oxide crystallizing technique using block copolymer micelles as vehicles for drug delivery[17, 18]. This drug delivery system has been used to deliver adriamycin to cancerous lesions[19]. It successfully accumulates adriamycin in the tumor by enhanced permeability retention effect[20]. With this system, the dose of adriamycin can be significantly reduced to obtain the same effect with less adverse effects. Similarly, our contrast medium apparently accumulated at the vascular lesion with increased permeability and successfully enhanced MR images of the lesion. We also found that T2 mapping is useful to detect small changes in T2 shortening in vascular lesions as well as the change induced by the accumulation of contrast medium at the site of increased permeability.

Materials and Methods

Block Copolymers

Poly (ethylene glycol) -poly (aspartic acid) block copolymer (CH_3 O (CH_2 CH_2 O)$_{272}$ CH_2 CH_2 CH_2 NH-(CHCOCH$_2$ COOHNH)$_{52}$H was prepared as reported previously[17]. The molecular weights of weight-average (Mw) and number-average (Mn) determined by Gel permeation chromatography (HLC-8220, TOSOH, Tokyo, Japan) were 17,560 and 15,990, respectively. The polydispersity index (Mw/Mn) was 1.098.

Novel Contrast Medium

Iron colloids were prepared by a new crystallization technique. Briefly, iron chloride $FeCl_3$ aqueous solution (0.1 mmol Fe/L) was stirred at 3℃ for one hour, aged at 50℃ for four hours and then at 20℃ for 48 hours. The iron colloid (0.1 mmol Fe/L) and the block copolymers (1 mg/mL) were mixed at room temperature for 24 hours[21].

Characterization of the Novel Iron Contrast Medium

Transmission electron microscopy was conducted with a LEO9220MEGA (Carl Zeiss Japan, Tokyo, Japan). Dynamic light scattering was performed with a Zetasizer nano S (Sysmex Japan, Tokyo, Japan). Relaxivity at 0.47 T was measured using a Minispec PC-20 spectrometer (Bruker Japan, Ibaragi, Japan). Two-pulse inversion recovery and the Carr-Purcell-Meiboom-Gill method were used for T1 and T2 measurements in water at 25℃.

Animals

Male Sprague-Dawley rats (six months old) were obtained from Clea Japan Co. Ltd (Tokyo, Japan). All animal experiments were performed according to the protocols approved by the Committee for Welfare and Ethics of Tokyo Medical and Dental University. Rats were anesthetized with pentobarbitone (30 mg/kg). The left carotid artery was injured with a 2F embolectomy catheter as reported previously[22]. After three weeks, the novel contrast medium (0.1 mmol Fe/kg) or ferumoxide (10 mmol Fe/kg) was injected into the tail vein. Rats were subjected to MR imaging under anesthesia with 1%-2% isoflurane.

Magnetic Resonance Imaging

MR images were obtained at 4.7 T with a Varian INOVA200 (Varian Technologies Japan Ltd., Tokyo, Japan) equipped with a quadrature coil. Carotid arteries were examined at ten slices (thickness: 2 mm, gap: 1 mm, field of view: 60×60 mm and matrix: 256×256) by a standardized spin echo protocol. Six different contrast-weighted images were obtained at each slice: proton density-weighted (TR/TE=2,500/8 ms) and a series of T2-weighted (TR/TE=2,500/12, 16, 20, 40, 80 ms). The images were obtained before and 1, 2, 4, 24 hours after injection of the contrast medium.

T2 Mapping

T2 relaxation time was calculated from these six spin-echo images by fitting a nonlinear least-squares curve to each voxel on the image, and a T2 mapping image was constructed by the Image Math program in Varian Browser software. The representation bar of T2 relaxation time was colored by Photoshop 7.0 (Adobe Systems Inc.) using a Macintosh computer. T2 relaxation time of each voxel was displayed according to the representation bar.

Histological Study

Rats were injected with Evans blue dye and perfused-fixed with 10% neutralized formalin. Paraffin-embedded sections of the carotid artery were stained with hematoxylin-eosin and Elastica van Gieson.